LITHOS 472–473 (2024) 107565

Contents lists available at ScienceDirect

LITHOS

journal homepage: www.elsevier.com/locate/lithos

# Bimodal volcanism in the Hegau region (SW Germany): Differentiation of primitive melilititic to nephelinitic rocks produces evolved nosean phonolites

Thomas Binder [a,*], Michael A.W. Marks [a], Brian-Eric Friedrichsen [a], Benjamin F. Walter [b], Thomas Wenzel [a], Gregor Markl [a]

[a] Department of Geosciences, Eberhard Karls Universität Tübingen, Schnarrenbergstraße 94–96, 72076 Tübingen, Germany
[b] Chair of Geochemistry & Economic Geology and Laboratory of Environmental and Raw Materials Analyses (LERA), Karlsruhe Institute of Technology, Adenauerring 20b, 76131 Karlsruhe, Germany

ARTICLE INFO

*Keywords:*
Bimodal volcanism
Central European Volcanic Province
Magmatic differentiation
Melilite-bearing olivine nephelinite
Mineral chemistry
Nosean phonolite

ABSTRACT

Peculiar bimodal volcanism in the Hegau region (SW Germany) comprises two contrasting $SiO_2$-undersaturated rock suites.

(I) Primitive olivine melilitites and melilite-bearing olivine nephelinites (12–9 Ma) are characterized by high MgO, CaO, $Fe_2O_3$, $TiO_2$, Ni, V, F, moderate alkalis, $Al_2O_3$, $P_2O_5$, Ba, Nb, Zr, and low $SiO_2$, Rb, Pb, and U concentrations. The rocks are composed of forsteritic olivine, diopsidic clinopyroxene, melilite, perovskite, Cr-bearing oxyspinel, F- and Ba-rich mica, and fluorapatite. In rare cases, they contain coeval coarse-grained ijolite patches generated by rapid in-situ fractionation in small melt pockets.

(II) Evolved nosean phonolites (14–11 Ma) comprise high alkalis, $Al_2O_3$, $SiO_2$, Rb, Nb, Zr, U, Pb, S, and low MgO, CaO, $Fe_2O_3$, $TiO_2$, $P_2O_5$, Ba, Ni, and V concentrations, and contain abundant Ba-bearing alkali feldspar and nosean-haüyne-sodalite$_{ss}$ macrocrysts, aegirine-augitic clinopyroxene, as well as accessory apatite, titanite, zircon, and pyrochlore.

The melilititic–nephelinitic rocks formed by low degrees of partial melting of a carbonated amphibole ± phlogopite-bearing garnet wehrlite in the uppermost asthenosphere or in the thermal boundary layer and occur also in neighbouring regions. However, their coexistence with evolved nosean phonolites is a unique and so far, unexplained feature in the southern Central European Volcanic Province.

Thermodynamic modelling implies that removal of 11–19% oxyspinel, 4–10% olivine, 42–57% clinopyroxene, <3% mica, <9% feldspathoids, <8% feldspar from melilititic–nephelinitic parental melts at upper crustal conditions (~200 MPa) results in significant amounts of phonolitic residues that are compositionally similar to the exposed nosean phonolites. Strongly negative P and Ti anomalies and a trough of MREE in primitive mantle-normalized trace element patterns of phonolites indicate additional fractionation of titanite and apatite, consistent with the mineralogy of coarse-grained (nepheline) syenitic cumulates, which are present as enclaves in both rock suites. The modelling results suggest crystallization of the (nepheline) syenite cumulates between 1050 and 800 °C and ascent and eruption of the phonolite residues at no less than ~900 °C with complete solidification of the observed assemblage at >750 °C. Significant crustal assimilation during fractionation appears unnecessary to explain the mineralogical, mineral chemical, and geochemical characteristics of the phonolites. Prolonged upper crustal differentiation of the magmas in one case (nosean phonolites) and fast ascent of primitive melts in the other (olivine melilitites and melilite-bearing olivine nephelinites) can be explained by stress field changes from an extensional to a more compressive regime, the magma ascent becoming thereby increasingly structurally controlled and supported by brittle deformation.

* Corresponding author.
*E-mail addresses:* thomas.binder@uni-tuebingen.de (T. Binder), michael.marks@uni-tuebingen.de (M.A.W. Marks), brian-eric.friedrichsen@student.uni-tuebingen.de (B.-E. Friedrichsen), b.walter@kit.edu (B.F. Walter), gregor.markl@uni-tuebingen.de (G. Markl).

https://doi.org/10.1016/j.lithos.2024.107565
Received 10 November 2023; Received in revised form 28 February 2024; Accepted 1 March 2024
Available online 7 March 2024

## 1. Introduction

Bimodal volcanism is characterized by the eruption of mafic and felsic lavas in the same volcanic region, and usually shows a lack of intermediately composed rocks (*Daly gap*; e.g., Berger et al., 2009; Freundt-Malecha, 2001; Zhao et al., 2023). Such districts are commonly associated with extensional regimes, especially continental but also oceanic rifts (e.g., Corti, 2009; Deering et al., 2011; Lacasse et al., 2007; Rooney, 2020; Trua et al., 1999) as well as arc and back-arc magmatism (e.g., Chen et al., 2018; Lexa et al., 2010; Tamura and Tatsumi, 2002).

Many concepts explaining bimodal rock suites involve different initial magma sources that occur either coincidentally or causally related in the same region, for example if the same geodynamic process causes partial melting of different lithologies and/or if the melting degree strongly varied in time, both of which produce different parental melts (e.g., Chen et al., 2018; Hoernle and Schmincke, 1993; Rooney et al., 2007; Zou and Zindler, 1996). Other models involve the well-known scenario of magmatic underplating, where ascending mafic magmas (mostly basalts or andesites) pond at the Moho or in the lower crust and provide heat and fluids that are transferred upward and facilitate partial melting of overlying felsic lithologies (producing mostly granites/rhyolites; e.g., Peccerillo et al., 2007; Tamura and Tatsumi, 2002; Trua et al., 1999).

In other cases, the felsic compositions are last products of a differentiation path (via fractional crystallization) of the primitive magma compositions of the same volcanic region (e.g., Berger et al., 2009; Kong et al., 2023; Peccerillo et al., 2007; Ulrych et al., 2003; Vaněčková et al., 1993; Wörner and Schmincke, 1984). Elsewhere, significant crustal assimilation is additionally required to derive evolved assemblages from primitive ones (Corti, 2009; Peccerillo et al., 2003; Rooney, 2020; Schmitt et al., 2017; Trua et al., 1999). The absence of exposed intermediate rocks in bimodal volcanic regions has been explained by high viscosity and/or density of intermediate magmas, preventing ascent and emplacement at or near the surface (Freundt-Malecha, 2001 and references therein). Other concepts assume a general suppression of formation of intermediate rocks, i.e., fractionation of predominantly mafic minerals first and mostly felsic minerals thereafter with only little overlap (Peccerillo et al., 2003 and references therein). Accordingly, the intermediate differentiation stage was exceeded within a narrow temperature interval and with a low crystallization rate for thermodynamic and geochemical reasons. However, plutonic enclaves in volcanic rocks support the existence of cumulates of intermediate composition in crustal magma chambers and sometimes minor volumes of intermediate rocks like trachyandesites, trachybasalts, phonotephrites, or tephriphonolites do occur (e.g., Anti-Atlas, East African Rift, Eger Graben, Canary Islands, Rhön, Siebengebirge; Berger et al., 2009; Corti, 2009; Freundt-Malecha, 2001; Jung et al., 2012; Jung et al., 2013; Sliwinski et al., 2015; Ulrych et al., 2005; Ulrych et al., 2011; Vaněčková et al., 1993; Zaitsev et al., 2012). Peccerillo et al. (2003) suggest that small quantities of intermediate, crystal-rich melts form a thin mushy interlayer between the mafic and felsic lithologies of a fractionating, continuously fed magma chamber and can be easily entrained, constituting plutonic enclaves in the melts while rarely erupting themselves.

The association of primitive mafic melilitites, foidites, or basanites with evolved felsic phonolites is particularly known from several regions in the Central European Volcanic Province (CEVP) and was explained by fractionation of olivine, oxyspinel, and clinopyroxene followed by plagioclase, sanidine, and sometimes amphibole, phlogopite, apatite, sodalite-haüyne-nosean$_{ss}$, titanite, and/or garnet in upper crustal magma reservoirs (e.g., Braunger et al., 2018; Büchner et al., 2015; Jung et al., 2013; Schleicher et al., 1990; Vaněčková et al., 1993; Wilson et al., 1995b; Wörner and Schmincke, 1984). In the Hegau region, the southernmost district of the CEVP (study area), however, cross-cutting relationships between primitive olivine melilitites to melilite-bearing olivine nephelinites and evolved nosean phonolites are missing. Furthermore, direct evidence for magma mixing or continuous fractionation trends that would manifest themselves in intermediate rocks are absent, as both rock suites occur in separate volcanic centres (cf. Fig. 1).

Except for scarce whole-rock analyses (von Engelhardt and Weiskirchner, 1961; Keller et al., 1990; Mahfoud and Beck, 1989), comprehensive mineral chemical and whole-rock geochemical analyses for the phonolites are still lacking. In the present study, extensive petrographic and mineral chemical data for the volcanic to subvolcanic rocks of the Hegau region (except for the tuffs) and their coarse-grained enclaves are presented and combined with fractional crystallization modelling using MELTS to shed light on the genetic relationship between primitive and evolved rocks and on the volcanic evolution in this area as a textbook example of Central European bimodal rock suites.

## 2. Geological setting

The Hegau volcanic region lies in SW Germany directly north of the High Rhine and northwest of Lake Constance with the NW-SE-trending, parallel Hegau and Überlinger See graben systems (Theilen-Willige, 2011). It is situated at the southeastern end of the Bonndorf Graben (Fig. 1a), which crosses the Schwarzwald and hits the Upper Rhine Graben (URG) in the west near Freiburg. The former three grabens are collectively known as Freiburg-Bonndorf-Bodensee Fault zone (FBBFZ; Egli et al., 2017). Additionally, the seismically active Albstadt shear zone (e.g., Ring and Bolhar, 2020) commences in the Hegau region and trends parallel to the URG, terminating immediately west of the Urach volcanic field, whose activity lasted from 19 to 12 Ma (Binder et al., 2023). Although major rifting processes occurred in the Miocene, post-Variscan, Paleozoic–Mesozoic precursor structures probably had a large impact on the recent fault systems in the ~15–25 km wide graben complex, possibly tapping the upper mantle by reactivation of deep-seated faults (Egli et al., 2017; Ring and Bolhar, 2020). This is supported by the length of the FBBFZ (~100 km), indicating a major crustal-scale deformation zone (Egli et al., 2017). Since the Early Miocene, graben formation has been intensified by NE-oriented extension and mainly NW-directed subvertical shortening (Ring and Bolhar, 2020).

The Hegau region is characterized by bimodal volcanism (Fig. 1a; Mahfoud and Beck, 1989; Mäussnest and Schreiner, 1982): In the north and west, ~25 isolated vents/necks and, more rarely, dykes of primitive olivine melilitites and melilite-bearing olivine-nephelinites (continuous transition, in the following referred to as melilitites–nephelinites) and tuffs of the same composition occur. In contrast, in the eastern central Hegau region, six prominent domes of evolved nosean phonolite dominate the landscape (Fig. 1b). Especially between these two volcanic fields and in the southeast, there are numerous mafic tuff vents and extensive tuff blankets, whose crystal load comprises mainly augite, hornblende, and phlogopite, and which are mostly lapilli tuffs.

As the southern CEVP predominantly comprises melilititic, foiditic, and basanitic rocks (Binder et al., 2023), the phonolites of the Hegau together with those from Katzenbuckel (Mann et al., 2006) and the Kaiserstuhl volcanic complex (KVC; e.g., Braunger et al., 2018) represent a peculiarity but are comparable to volcanic rocks from the French Massif Central (Wilson et al., 1995a and references therein). Based on geochronology (Binder et al., 2023), the olivine melilitites and melilite-bearing olivine nephelinites, and ijolitic patches therein (12–9 Ma) are the youngest rocks (of the entire southern CEVP), whereas the nosean phonolites are slightly older (14–11 Ma). Syenite and nepheline syenite enclaves in the phonolites, in the melilititic–nephelinitic rocks, and in the mafic tuffs show the same age range (15–11 Ma). The primitive melilitites–nephelinites of the Hegau region were produced by low-degree partial melting of an amphibole ±phlogopite-bearing garnet peridotite in the uppermost asthenosphere or the lower lithospheric thermal boundary layer, which underwent $CO_2$- and Ca-rich subduction-related metasomatism (Alibert et al., 1983; Binder et al., 2024; Blusztajn and Hegner, 2002; Dunworth and Wilson, 1998; Hegner and Vennemann, 1997). Mobilization, infiltration, and emplacement of

metasomatic agents probably occurred in consequence of continuous dehydration and recycling of Variscan oceanic lithosphere, comprising the release of Ca-rich carbonates, further volatiles, and incompatible elements into the mantle (Binder et al., in press).

Graben and basin fillings of the Hegau region consist of Oligocene–Miocene Alpine molasse sediments, and are underlain by Upper Jurassic limestones (Schreiner, 2008). The deposition of conglomerates (17–15 Ma) and particularly the *Juranagelfluh* sediments (<15 Ma) reflect an important stage of erosion and unroofing in the Alpine foreland as a result of pronounced uplift of the Vosges-Swabian arc (Ring and Bolhar, 2020). Bedding inclines to the southeast at up to 5° due to gradually increasing subsidence caused by the loading of the Alpine orogen (Egli et al., 2017). Distinct step faults on the southwestern flanks of the Hegau Graben system reach into the basement and dip subvertically to subhorizontally to the NE (e.g., Randen, Schienerberg faults; Fig. 1a), adding up to an offset of ~300 m, while northeastern graben faults are less well defined and dip SW, displaying a maximum offset of ~120 m (Mindelsee fault; Fig. 1a; Egli et al., 2017; Schreiner, 2008). The wedge-like sedimentary sequence thickens from the NW basin edge to 1600 m at the western end of Lake Constance (Schreiner, 2008).

## 3. Material and methods

For petrographic examination, 44 thin sections from 23 localities of the Hegau region were available (Table 1). The samples originate from collections of the University of Tübingen and the LGRB Freiburg (Germany); in addition, several localities were resampled to augment the inventory. All thin sections were studied by light microscopy and scanning electron microscopy (*Phenom XL, Thermo Fisher Scientific*) at the Department of Geosciences, University of Tübingen. A subset of the samples was used in the geochronological and petrological studies of Binder et al. (2023) and Binder et al. (in press). For the present study, 15 samples (ijolite, nosean phonolite, nepheline syenite, syenite) from seven localities (Table 1) were selected for electron probe microanalysis (EPMA).

### 3.1. Whole-rock geochemistry

Whole-rock analyses (major, minor, and trace elements) of twelve fresh to weakly altered samples from all six nosean phonolite domes of the Hegau region (Table 1) were performed at the Laboratory of Environmental and Raw Materials Analysis (LERA, Institute for Applied Geosciences), Karlsruhe Institute of Technology (Germany), using wavelength dispersive XRF (*S4 Explorer, Bruker AXS*) and ICP-MS (*iCap RQ, Thermo Fisher Scientific*). The data protocol given in the Supplementary data, File 1 comprises the analyses of the reference material, reference values for the standards, deviations from the reference values, acid blind analyses and their 1σ. To determine the mass loss on ignition, one gram of the powdered sample was heated to 950 °C for 3 h. For XRF, fused beads were prepared with a Li tetraborate/metaborate mixture (*Spectroflux 110, Alfa Aesar*) as flux. The certified standards AGV-1 (andesite), GS-N (granite), SY-2 and SY-3 (syenites) were measured intermittently as secondary reference materials during the same session as our samples (Govindaraju, 1994; CRM-TMDW-A, *High-Purity standards, Inc.*), yielding an accuracy in the range of 2.5% for most elements and 8% for Ti and Mn relative to sample composition.

For ICP-MS, 100 mg of powdered rock was treated by $HNO_3$-HF-$HClO_4$ acid digestion. A sample was heated together with 65% $HNO_3$ (subboiled), 40% HF (Suprapur®), and 65% $HClO_4$ (Normatom®) in a closed Teflon vessel for 16 h at 120 °C, assuring a total silicate decomposition. After evaporating the acids to incipient dryness, the residue was redissolved in 65% $HNO_3$ (subboiled) and evaporated again (three times) for purification purposes. The final residue was dissolved in 50 mL of ultrapure $H_2O$. The quality of the ICP-MS trace element analyses was ensured by including the two certified reference materials SY-2 and SY-3 (Govindaraju, 1994), an in-house phonolite standard, and two

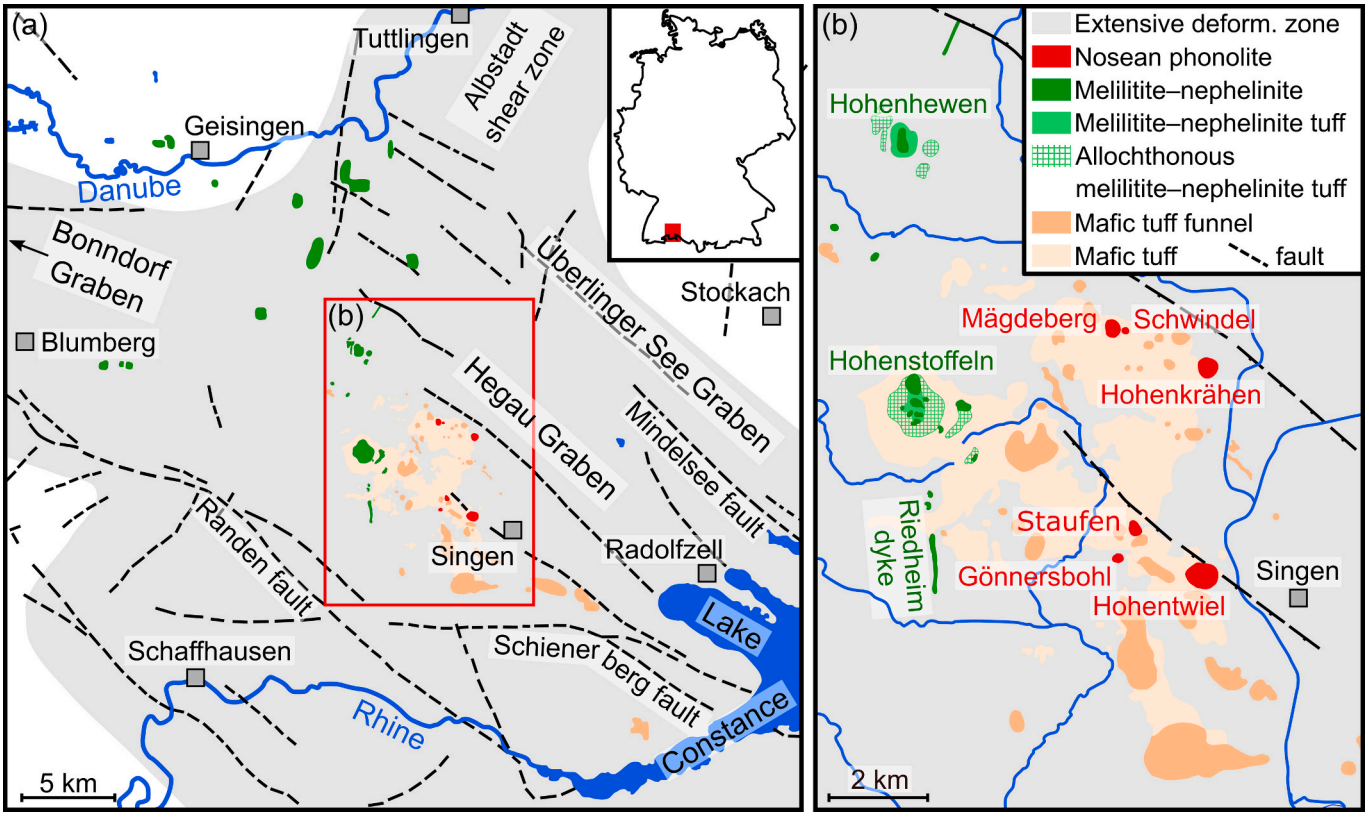


**Fig. 1.** (a) Simplified map of the Hegau region showing the different volcanic rock units and major fault structures (after Egli et al., 2017). (b) Enlarged section of the central Hegau region with its melilititic–nephelinitic vents in the west and phonolite domes in the east. Large areas in between are covered by mafic tuffs.

**Table 1**
Sample list including locality name, coordinates, and rock type.

| Sample | Locality | Latitude (°N) | Longitude (°E) | Rock type |
|---|---|---|---|---|
| HEG 10 | Blauer Stein (Randen) | 47.825537 | 8.597696 | Nph & Hyn b. ol melilitite |
| HEG 12 | Blauer Stein (Randen) | 47.825537 | 8.597696 | Mll-b. olivine nephelinite |
| N 374 | Blauer Stein (Randen), Steinröhren | 47.826987 | 8.598313 | Mll-b. olivine nephelinite |
| HEG 01, HEG 01a | Haslen | 47.814300 | 8.760884 | Olivine melilitite |
| HEG 03a | Hohenstoffeln | 47.794465 | 8.750537 | Mll-b. olivine nephelinite |
| HEG 04 | Hohenstoffeln | 47.794465 | 8.750537 | Nepheline olivine melilitite |
| HEG 13 | Homboll | 47.784160 | 8.764518 | Nph-b. olivine melilitite |
| N 333 | Höwenegg | 47.914362 | 8.738509 | Nepheline olivine melilitite |
| HEG 15 | Neuhewen | 47.879057 | 8.717537 | Mll-b. olivine nephelinite |
| N 323 | Neuhewen | 47.879056 | 8.717029 | Olivine melilitite |
| HEG 19 | Pfaffwiesen | 47.776275 | 8.752612 | Mll-b. olivine nephelinite |
| N 593 | Ramsen | 47.817302 | 8.731386 | Mll-b. olivine nephelinite |
| HEG 20 | Riedheim dyke | 47.763659 | 8.753926 | Nepheline olivine melilitite |
| HEG 14 | Schachen | 47.821626 | 8.730429 | Mll & Hyn b. ol nephelinite |
| HEG 18 | Sennhof | 47.789871 | 8.755671 | Olivine melilitite |
| I 27 | Tudoburg | 47.879076 | 8.883742 | Mll-b. olivine nephelinite |
| HEG 16, HEG 11, I 224 | Wartenberg | 47.915868 | 8.631607 | Mll-b. olivine nephelinite |
| I 63 | Wasserburger Tal | 47.900917 | 8.871255 | Mll-b. olivine nephelinite |
| N 290 | Wasserburger Tal | 47.876242 | 8.845515 | Mll-b. olivine nephelinite |
| HEG 02 | Hohenstoffeln | 47.794465 | 8.750537 | Ijolite |
| HEG 03 | Hohenstoffeln | 47.794465 | 8.750537 | Mll-b. ol nephelinite, ijolite |
| HEG 05 | Hohenstoffeln (EPMA) | 47.794465 | 8.750537 | Ijolite |
| HEG 17 | Hohenhewen | 47.835623 | 8.747227 | Mll-b. ol nephelinite, ijolite |
| GB-1 | Gönnersbohl (EPMA, WR) | 47.767451 | 8.798665 | Nosean phonolite, syenite |
| GB-2 | Gönnersbohl (EPMA) | 47.767451 | 8.798665 | Nosean phonolite, syenite |
| GB-3 | Gönnersbohl | 47.767451 | 8.798665 | Nosean phonolite, syenite |
| HG-1 | Hohentwiel (EPMA) | 47.764720 | 8.818884 | Nosean phonolite |
| HK-1 | Hohenkrähen (EPMA, WR) | 47.798777 | 8.820079 | Nosean phonolite |
| HK-2 | Hohenkrähen (EPMA, WR) | 47.798777 | 8.820079 | Nosean phonolite |
| HW-1 | Hohentwiel (WR) | 47.764720 | 8.818884 | Nosean phonolite, syenite |
| HW-2 | Hohentwiel (EPMA, WR) | 47.764720 | 8.818884 | Nosean phonolite, syenite |
| HW-2a | Hohentwiel (EPMA) | 47.764720 | 8.818884 | Nosean phonolite, syenite |
| HW-3 | Hohentwiel (EPMA, WR) | 47.764720 | 8.818884 | Nosean phonolite |
| MB-1 | Mägdeberg (EPMA) | 47.805260 | 8.797495 | Nosean phonolite |
| MB-2 | Mägdeberg (WR) | 47.805260 | 8.797495 | Nosean phonolite |
| MB-3 | Mägdeberg (WR) | 47.805260 | 8.797495 | Nosean phonolite |
| MB-4 | Mägdeberg (EPMA, WR) | 47.805260 | 8.797495 | Nosean phonolite |
| SCH-1 | Schwindel (EPMA, WR) | 47.805017 | 8.800298 | Nosean phonolite |
| ST-1 | Staufen (EPMA, WR) | 47.771704 | 8.806615 | Nosean phonolite |
| ST-2 | Staufen (EPMA, WR) | 47.771704 | 8.806615 | Nosean phonolite |
| HEG 06 | Hohenstoffeln (EPMA) | 47.794465 | 8.750537 | Nepheline syenite |
| HEG 08 | Hohenstoffeln | 47.794465 | 8.750537 | Syenite |
| E 403 | 2 km E Weil | 47.817306 | 8.731385 | Nepheline syenite |
| N 248 | 2 km E Weil | 47.817306 | 8.731385 | Nepheline syenite |

b. – bearing; EPMA – electron probe microanalyses performed on the sample for this study; Hyn – haüyne; Mll – melilite; Nph – nepheline; Ol – olivine; WR – whole-rock analysis performed on the sample.

blank samples into the protocol. The accuracy relative to sample composition was 10% for most trace elements, except for Sc, Cr, Ni, Cs, Hf, Ta, W, and some HREEs (25%).

The contents of total C and S were determined by combusting powdered material in an $O_2$ flow with an induction furnace at 2000 °C (*CS 2000, Eltra*). The reference materials steel ($n = 7$) and cast iron ($n = 2$) were used for calibration and quality control. Accuracy relative to sample composition was in the range 1%; the 1σ was 0.7% for steel, 2.5% for cast iron.

### 3.2. EPMA

The mineral chemistry was determined using a *JEOL JXA 8230* electron probe microanalyzer in wave-length dispersive mode at the Department of Geosciences, University of Tübingen. Depending on the composition of the minerals, different configurations (acceleration voltage, probe current, probe diameter) were applied (Supplementary data, Table A1). The specific sensitivities of the mineral surface to the probe current were a critical factor when performing the adjustments. Peak count times were fixed at 10 s for light and volatile elements in clinopyroxene, perovskite, apatite, and amphibole (Na, F), 16 s for the other major elements, and 30 s for minor elements, with background count time being each half of peak count time. The calibration was carried out by using synthetic and natural reference materials, and by application of several peak overlap corrections (Cr—V, V—Ti, F—Fe, F—Ce, Ce—Ba, Pr—La, Ba—Ti). An internal φ(ρz) raw data correction was performed for all analyses except oxyspinel and ilmenite analyses, for which ZAF correction was applied. Specific parameters for the analytical protocols are given in Supplementary data, Tables A2–8, details of mineral formula and endmember calculations in Supplementary data, File 2, and all analytical results in File 3. The results of the mineral chemical analyses performed in this study are supplemented by data from nine localities of melilitites–nephelinites from the Hegau region (Binder et al., in press).

### 3.3. Fractionation modelling using MELTS

Using the easyMELTS graphical user interface (version 0.2.4) of the MELTS software platform (Ghiorso and Sack, 1995), fractional crystallization of the primitive melilititic–nephelinitic Hegau magmas was modelled based on the thermodynamic database and algorithms provided in the rhyolite-MELTS 1.2.0 version (Ghiorso and Gualda, 2015; Gualda et al., 2012). This version is optimised for crystallization in bulk compositions at 0–3 GPa that are not saturated with quartz, considering

also the $H_2O$-$CO_2$ fluid saturation model of Ghiorso and Gualda (2015). It represents the best approximation of the MELTS software package for fractional crystallization of mafic alkaline $SiO_2$-undersaturated magmas at crustal depths and was successfully tested for very similar rock types (Kong et al., 2023; Mourey et al., 2023; Sliwinski et al., 2015 and references therein). The isothermal computation mode for each individual step and a temperature increment of −10 K were used for the modelling, while the pressure was set constant (cf. Supplementary data, File 4). Only solids were considered as fractionating phases and the $fO_2$ buffer was set to ΔFMQ +3, based on thermodynamic modelling for these rocks (Binder et al., in press) and because Braunger et al. (2018) determined a similarly high ΔFMQ of +2 to +3 for the KVC olivine nephelinites. All available whole-rock analyses of melilititic–nephelinitic rocks of the Hegau region (Supplementary data, File 1) were used as input data to largely cover the entire geochemical range of conceivable parental magma compositions. These span $H_2O$ contents from 0.0 to 3.9 wt% (Supplementary data, Fig. A1) and $CO_2$ contents from 0.0 to 0.2 wt%, extending beyond the ranges of other work dealing with MELTS modelling of alkaline rocks (Mourey et al., 2023; Sliwinski et al., 2015). Note, however, that modelling was not applicable to some whole-rock compositions and resulted in a software error (see Discussion for details). The calculations were performed assuming crustal pressures of 200, 500, and 1000 MPa during fractional crystallization (cf. Kong et al., 2023; Mourey et al., 2023). The modelled evolution of the residual melt composition was compared with whole-rock data for the Hegau phonolites (this study; Alibert et al., 1983; Dunworth and Wilson, 1998; von Engelhardt and Weiskirchner, 1961; Keller et al., 1990; Krause, 1969; Krause and Weiskirchner, 1981; Staesche, 1995; Stock, 1990; Wimmenauer, 1974).

## 4. Results

### 4.1. Petrography

Based on mineral assemblages (Table 2) and (micro)textures, primitive melilititic–nephelinitic, evolved phonolitic rocks, and coarse-grained ijolitic patches and (nepheline) syenite enclaves were distinguished.

#### 4.1.1. Olivine melilitites and melilite-bearing olivine nephelinites

These porphyritic rocks contain high amounts of olivine macrocrysts (20–40 vol%), comprising variable proportions of euhedral to subhedral crystals and subhedral to anhedral, rounded, partly sheared, ruptured crystals, which occasionally exhibit wavy extinction. A separation of the different types is not always univocal, as transitions in habitus and crystal size may be blurred (Figs. 2a & b). Further, the rocks show tabular to lath-shaped, yellowish–reddish brown euhedral clinopyroxene macrocrysts (5–20 vol%), and small melilite crystals (<10 vol%; Figs. 2a & b) embedded in a groundmass of euhedral clinopyroxene (10–35 vol%), titanomagnetite (10–15 vol%), melilite (<20 vol%), olivine (<10 vol%), interstitial nepheline (<20 vol%), and accessory euhedral perovskite and apatite. Clinopyroxene often shows concentric and/or hourglass sector zoning and rarely, pale, partly resorbed and inclusion-rich cores are present. Some samples contain anhedral dark mica (<5 vol%; Fig. 2a), euhedral medium-grained haüyne macrocrysts (<5 vol%; Fig. 2a & b), and/or clinopyroxene glomerocryts (Fig. 2a).

#### 4.1.2. Ijolites

Coarse-grained and irregularly shaped ijolitic patches within the melilites–nephelinites are delimited by a few millimetres wide transition zone that bridges the difference between the two rock types regarding composition and texture (Fig. 2c). The ijolite is characterized by a parquet texture of tabular euhedral to subhedral nepheline and its alteration products (50–60 vol%; Figs. 2d-f) and euhedral reddish or greenish brown clinopyroxene (~30 vol%) that is mostly concentrically (Fig. 2e) and/or hourglass sector zoned (Fig. 2f). These minerals are accompanied by medium-grained, squat or skeletal titanomagnetite (~10 vol%; Figs. 2d, e & g), euhedral apatite (Fig. 2f & g), interstitial carbonate (Fig. 2d), purple skeletal crystals and crystal groups of perovskite (Figs. 2g & h), and subordinate subhedral to anhedral dark mica (Fig. 2e).

#### 4.1.3. Nosean phonolites

The phonolites are characterized by large macrocrysts of euhedral nosean-haüyne-sodalite$_{ss}$ (10–25 vol%), with deep blue irregular shaped domains representing the S-rich primary composition of this sodalite-group mineral (see below) and light glaucous nosean-rich areas (Figs. 3a & b). A second population of medium-sized crystals exhibits only these paler colours (Figs. 3a & b) and many crystals of nosean-haüyne-sodalite$_{ss}$ are completely altered (Fig. 3c). Other macrocrysts are euhedral medium-grained yellow or yellowish green to bottle-green clinopyroxene (<10 vol%; Figs. 3c & d; mostly aegirine-augite), alkali feldspar of variable size (<25 vol%; Fig. 3c & e), and occasional rhombical titanite (Fig. 3c) that rarely shows twinning (Fig. 3e). Common accessories are euhedral to subhedral apatite (Fig. 3e; occurring also in crystal groups, Fig. 3f), zircon, and pyrochlore. All these minerals are embedded in a groundmass (50–80 vol%) of alkali feldspar, nosean, nepheline, and aegirine-augite (Figs. 3a-e).

#### 4.1.4. Syenites and nepheline syenites

Coarse-grained syenite and nepheline syenite enclaves occur in the phonolites (Fig. 4a) and in the melilititic–nephelinitic rocks. They are mineralogically similar but vary in terms of the mineral proportions, sometimes within the same enclave (Fig. 4b). The rocks consist of tabular euhedral to subhedral alkali feldspar (50–65 vol%; Figs. 4b-g), nepheline (<35 vol%; Figs. 4d & e), euhedral to subhedral clinopyroxene (<30 vol%; aegirine-augite; Figs. 4a-c, f & g), subhedral to anhedral dark mica (<5 vol%; Figs. 4b-g), interstitial carbonate (Figs. 4e-g), and

**Table 2**
Sample list including locality name, coordinates, and rock type. Modal mineralogy of investigated volcanic rocks in the Hegau region. Distinctive values are in grey, characteristic accessories are in bold.

| Rock series | Ol | Cpx | Spl/ Usp | Bt/ Phl | Mll | Nph +Zeo | Hyn/ Nsn/Sdl | Afs | Acc. |
|---|---|---|---|---|---|---|---|---|---|
| Olivine melilitites and melilite-bearing nephelinites | 20–40 | 10–35 | 10–15 | <5 | <20 | <20 | < 5 | – | **Prv,** Ap |
| Ijolites | – | ~30 | ~10 | Acc. | – | 50–60 | – | – | **Prv, Ap** |
| Nosean phonolites | – | 10–20 | Acc. | Acc. | – | 15–30 | 15–25 | 40–50 | **Ttn, Ap,** Zrn, Pcl |
| Syenites and nepheline syenites | – | <30 | Acc. | < 5 | – | <35 | – | 50–65 | **Ttn, Ap** (<30 vol.%!), **Zrn, Pcl,** Tho, Thr |

Ol – olivine; Cpx – clinopyroxene; Spl – spinel group (including magnetite); Usp – ulvöspinel; Bt – biotite; Phl – phlogopite; Mll – melilite; Nph – nepheline; Zeo – zeolites; Hyn – haüyne; Nsn – nosean; Sdl – sodalite; Afs – alkali feldspar; Acc. – accessory minerals; ap – apatite; prv – perovskite; ttn – titanite; zrn – zircon; pcl – pyrochlore; tho – thorianite; thr – thorite.

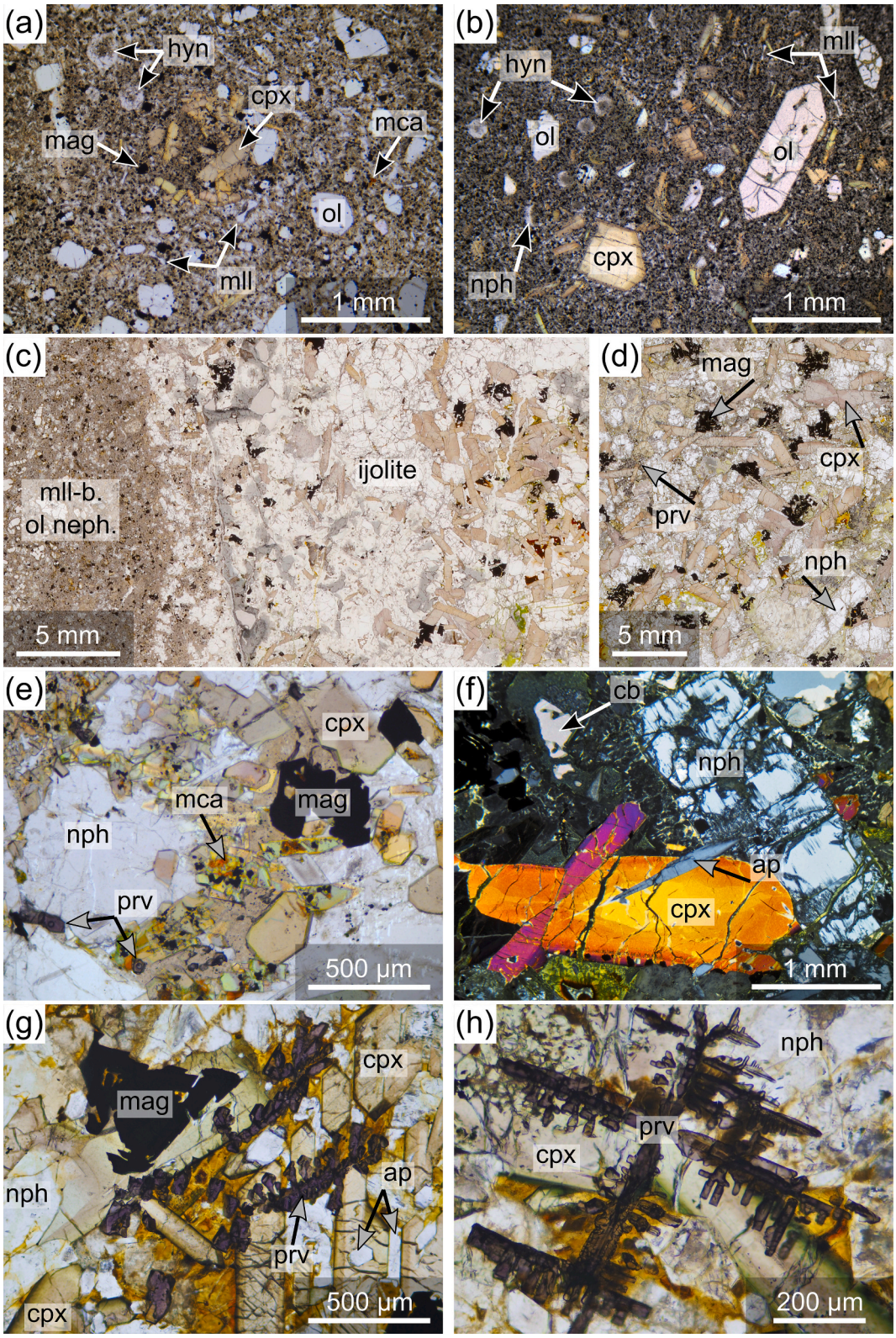


**Fig. 2.** Petrographic features of the Hegau melilitites–nephelinites and ijolitic patches therein. (a) Nepheline- and haüyne-bearing olivine melilitite with olivine and haüyne macrocrysts and clinopyroxene glomerocryts in fine-grained groundmass with accessory dark mica (Blauer Stein). (b) Nepheline-bearing olivine melilitite with olivine and zoned clinopyroxene macrocrysts, euhedral haüyne, and subhedral nepheline in fine-grained groundmass (Homboll). (c) Border zone between melilite-bearing olivine nephelinite and irregularly shaped ijolite patch (Hohenstoffeln). (d) Ijolite with tabular nepheline, euhedral reddish-brownish and greenish-brownish clinopyroxene, skeletal magnetite, and skeletal perovskite (Hohenstoffeln). (e) Ijolite-like textures with tabular nepheline, euhedral reddish-brownish and greenish-brownish clinopyroxene, skeletal magnetite, little perovskite, and dark mica within a melilite-bearing olivine nephelinite (Hohenhewen). (f-h) Ijolite (Hohenstoffeln) with (f) euhedral tabular nepheline, sector- and concentrically zoned subhedral clinopyroxene, needles and hexagonal cross-sections of apatite, and interstitial carbonate (crossed polarization), (g) euhedral–subhedral skeletal perovskite and magnetite crystals accompanied by tabular nepheline and euhedral clinopyroxene and apatite crystals, and (h) euhedral skeletal perovskite surrounded by clinopyroxene and nepheline.

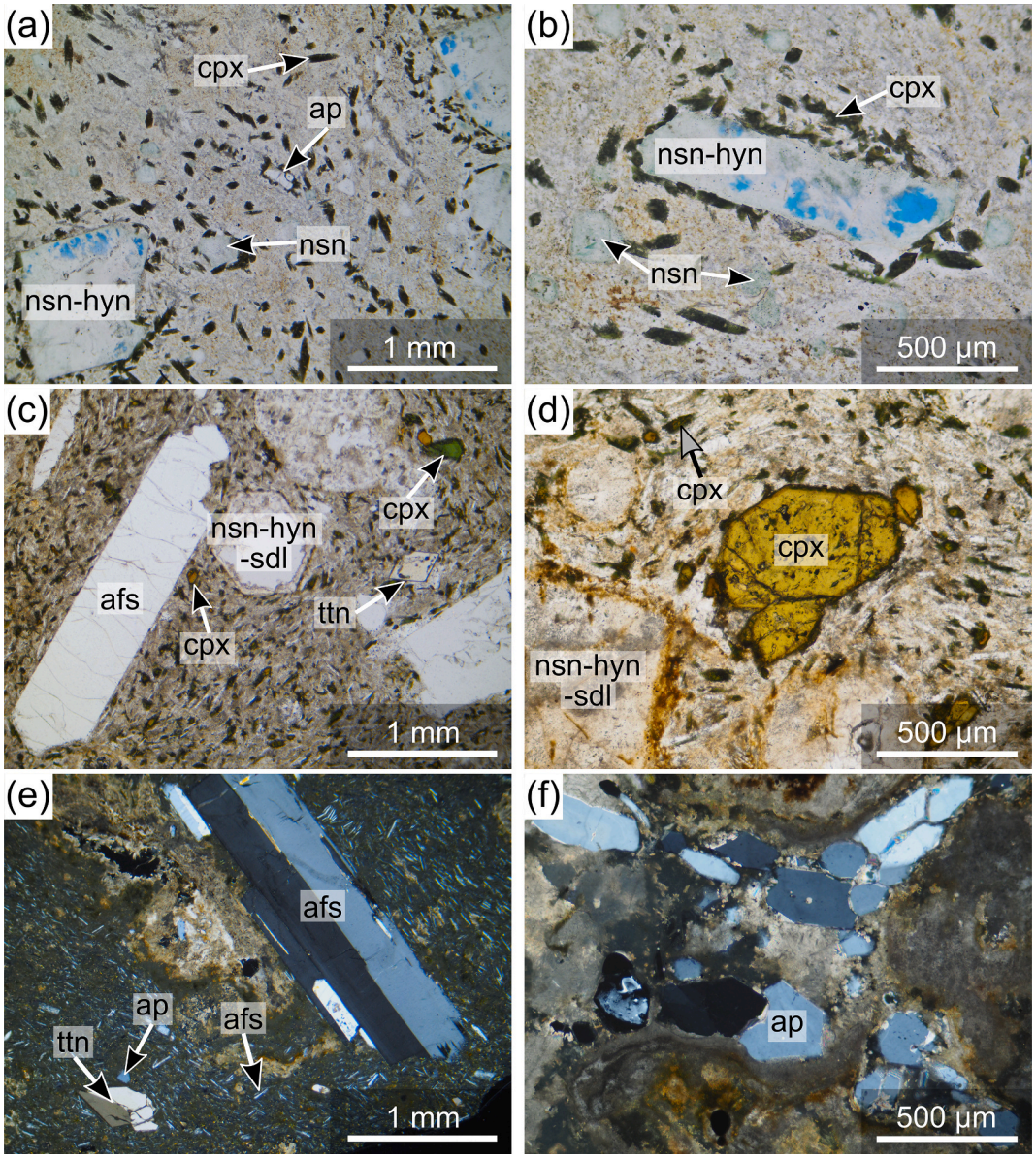


**Fig. 3.** Petrographic features of the Hegau nosean phonolites with (a) altered euhedral sodalite-group macrocrysts showing exsolution textures (of mainly haüyne-nosean$_{ss}$) in a groundmass of clinopyroxene (aegirine-augite), alkali feldspar, nepheline, sodalite-group minerals, and apatite (Hohenkrähen), (b) altered nosean crystals and a tabular euhedral macrocryst of exsolving haüyne-nosean$_{ss}$ fringed by small euhedral–subhedral clinopyroxene (aegirine-augite) microcrysts within a fine-grained grundmass of alkali feldspar, nepheline, and aegirine-augite (Hohenkrähen), (c) macrocrysts of alkali feldspar, a strongly altered sodalite-group mineral, titanite, and clinopyroxene in a groundmass of alkali feldspar, aegirine-augite, and nepheline (Hohentwiel), (d) macrocrysts of clinopyroxene and strongly altered haüyne-nosean-sodalite$_{ss}$ in a groundmass of euhedral–subhedral alkali feldspar, clinopyroxene, and nepheline (Hohenkrähen), (e) a twinned alkali feldspar macrocryst, a euhedral titanite crystal and microcrysts of apatite and alkali feldspar in a cryptocrystalline groundmass of clinopyroxene, alkali feldspar, and nepheline (crossed polarization; Hohentwiel), and (f) an agglomeration of euhedral–subhedral apatite crystals within a strongly altered groundmass (crossed polarization; Hohentwiel).

minor opaque phases. Few samples contain up to 30 vol% apatite, others only accessory amounts. Further accessories are euhedral titanite (Figs. 4f & g), irregularly or concentrically zoned pyrochlore (Figs. 4h-j), and zircon (Figs. 4e-g & k). Rarely, thorite and thorianite occur, sometimes as small inclusions in zircon (Fig. 4k).

### 4.2. *Whole-rock geochemistry*

Consistent with mineralogy, most melilitites–nephelinites plot in the lower part of the foidite/melilitite field in the TAS diagram (Fig. 5). However, some occurrences have slightly elevated $SiO_2$ contents classifying them as picrobasalts, rarely as tephrites or basanites. Nosean phonolites fall within the range of phonolites in the TAS diagram, except for four analyses with slightly lower $Na_2O + K_2O$ contents defining them as tephriphonolite, trachyandesite, or trachyte.

Major and trace element compositions (Figs. 6–7; Supplementary data, File 1) show clear differences between the various rock types in the Hegau region. The melilitites–nephelinites show high MgO contents (10–20 wt%), while the ijolitic patches therein have a content of only 7 wt% and the phonolites below 1.1 wt% MgO. $Na_2O + K_2O$ contents are low in the melilititic–nephelinitic rocks, slightly elevated in the ijolite, and high in the phonolites (Fig. 6a), whereas the opposite is observed for CaO, with the ijolite having the same contents as the primitive rocks (Fig. 6b). $Al_2O_3$ contents are moderate in the melilititic–nephelinitic rocks, mildly increased in the ijolite, and high in the phonolites (Fig. 6c). Likewise, the $SiO_2$ content is lowest in the ijolite and in the primitive

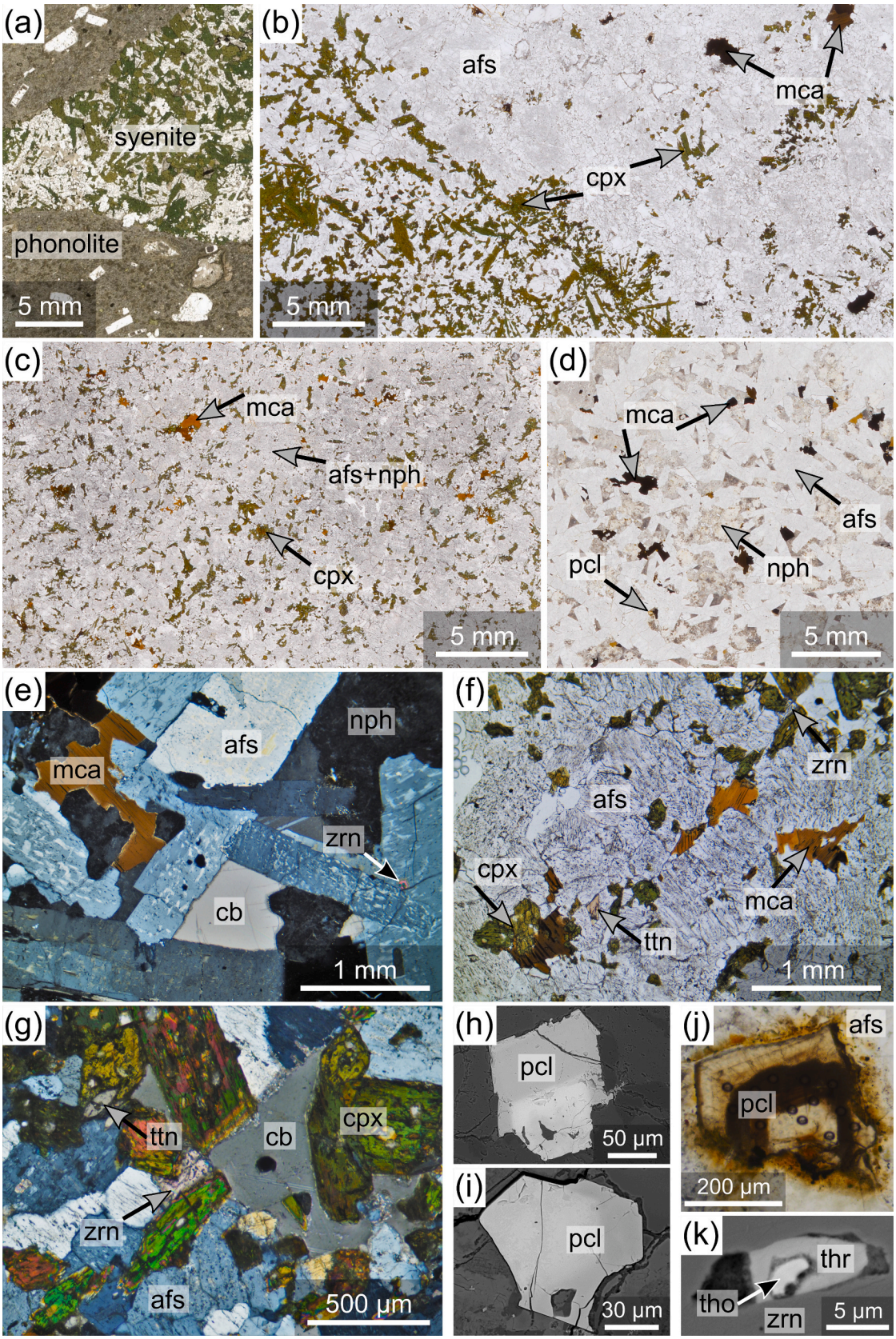


*(caption on next page)*

**Fig. 4.** Petrographic features of the Hegau (nepheline) syenites. (a) Syenite enclave within a nosean phonolite (Gönnersbohl). (b) Syenite with a mesocratic domain of clinopyroxene (aegirine-augite), alkali feldspar, and subordinate dark mica and a leucocratic domain of alkali feldspar, dark mica, and subordinate clinopyroxene (Hohenstoffeln). (c) Mesocratic nepheline syenite with alkali feldspar, nepheline, clinopyroxene (aegirine-augite), and dark mica (Hohenstoffeln). (d + e) Leucocratic nepheline syenite from a mafic tuff (2 km E Weil) with (d) alkali feldspar, nepheline, dark mica, and accessory pyrochlore and (e) tabular euhedral–subhedral alkali feldspar – exhibiting exsolved irregular perthite intergrowth –, anhedral tabular dark mica, altered nepheline, interstitial carbonate, and accessory zircon; crossed polarization. (f + g) Mesocratic nepheline syenite enclave from a nepheline-bearing olivine melilitite (Hohenstoffeln) with (f) subhedral–anhedral tabular alkali feldspar, clinopyroxene, dark mica, and accessory euhedral titanite and anhedral zircon and (g) tabular euhedral–subhedral clinopyroxene, subhedral alkali feldspar, interstitial carbonate, and accessory euhedral titanite and anhedral zircon; crossed polarization. (h + i) BSE images show chemically zoned pyrochlore microcrysts with (h) concentric zoning and (i) irregular–diffuse zoning, each due to differences in the U-Th-REE concentrations (nepheline syenite enclave from mafic tuff 2 km E Weil). (j) Concentrically chemically zoned pyrochlore microcryst with U-Th-rich metamict domains and transparent Nb-dominated zones embedded in alkali feldspar (2 km E Weil). (k) BSE image shows an inclusion of thorianite within an inclusion of thorite within a zircon crystal (nepheline syenite enclave from a nepheline-bearing olivine melilitite, Hohenstoffeln).

rocks and highest in the phonolites (Fig. 6d). $Fe_2O_3$, $TiO_2$, and $P_2O_5$ contents strongly decrease from the primitive rocks towards the evolved ones (Figs. 6e-g). The ijolite, however, exhibits the highest $P_2O_5$ concentrations (Fig. 6g). The Na/K ratio varies considerably in the melilitites–nephelinites and in the phonolites but decreases on average as the rocks evolve (Fig. 6h).

The Cr and Ni concentrations are high in the primitive rocks and decrease with decreasing MgO contents, whereas they are very low in the phonolites (Fig. 7a-b). Moderate Nb and Zr and high V concentrations in the melilititic–nephelinitic rocks contrast high Nb and Zr and moderate V contents in the evolved rocks (Fig. 7b-d). Rb, Pb, and U concentrations are significantly higher in the phonolites than in the primitive rocks (Fig. 7f-h).

Compared to the primitive mantle (Fig. 8a; Palme and O'Neill, 2014), the melilititic–nephelinitic rocks are strongly enriched in LREE (~80–130 times) but only slightly enriched in HREE (~2.5–5 times). The phonolites also show high enrichment for LREE (~45–150 times) and only moderate enrichment for HREE (~3–7 times), but additionally exhibit a trough for MREE (~2.5–13 times), whereas the primitive volcanic rocks are more enriched in these elements (~7–20 times). The primitive mantle-normalized trace element patterns show decreasing enrichment with increasing mantle compatibility in all volcanic Hegau rocks, albeit there are prominent exceptions (Fig. 8b). The melilititic–nephelinitic rocks have negative Rb, K, Pb, and positive Nb and P anomalies. In contrast, the phonolites reveal prominent positive U, Nb, and Zr anomalies and negative Ta, P, and Ti anomalies, while the K anomaly is absent and a slight positive Pb anomaly present.

### 4.3. Mineral chemistry

#### 4.3.1. Clinopyroxene

Clinopyroxene in the melilitites–nephelinites is generally unzoned and dominated by quadrilateral end-members (>60%; mostly Di + Hd; Fig. 9a), with varying tschermakitic components (<40%; FeTs, CaTiTs, CaAlTs, CrAlTs) and only ~5% Na pyroxene (Aeg, Ti-Aeg, Jd). In the ijolitic patches, clinopyroxene is similar in composition, with crystal rims, however, exhibiting higher proportions of Na pyroxene (up to 21%) at low Tschermak's substitution (<8%). In contrast, clinopyroxene

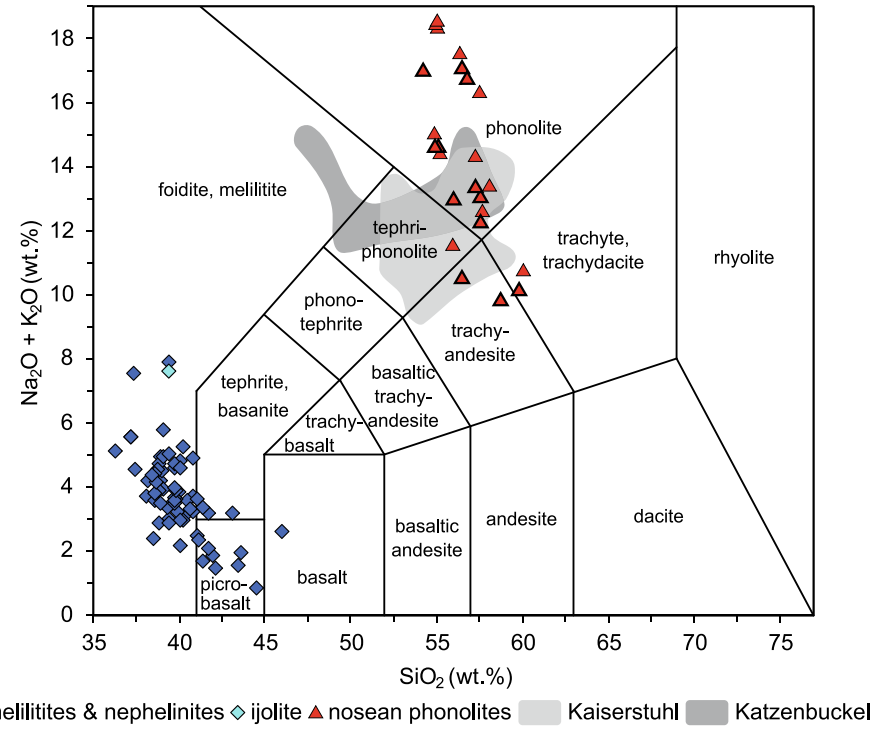


**Fig. 5.** TAS diagram showing compositions of the volcanic Hegau rocks. 12 new analyses (black-rimmed triangles) were supplemented by literature data from Alibert et al. (1983), Dunworth and Wilson (1998), von Engelhardt and Weiskirchner (1961), Keller et al. (1990), Krause (1969), Krause and Weiskirchner (1981), Staesche (1995), Stock (1990), and Wimmenauer (1974). All data have been renormalized to a volatile-free composition. For comparison, the compositions of the other phonolites of the southern CEVP are shown, namely those of the Kaiserstuhl (Braunger et al., 2018 and references therein) and Katzenbuckel (Frenzel, 1975; Freudenberg, 1906; Stähle and Koch, 2003). The naming of the rocks in the Petrography chapter is based on mineral compositions, so the position in the TAS diagram may differ from the assigned rock name.

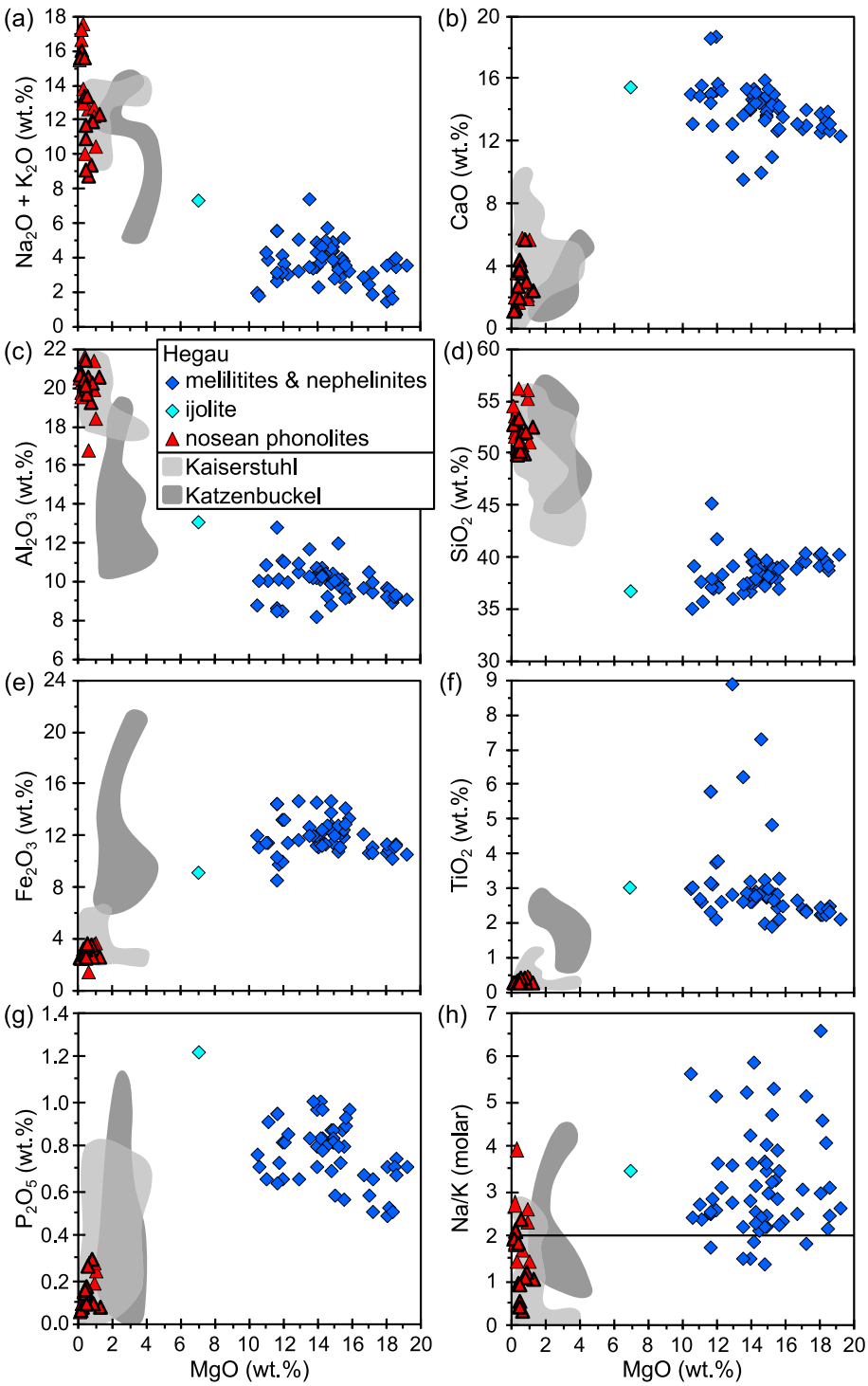


**Fig. 6.** Whole-rock major element composition of the igneous Hegau rocks. 12 new analyses (black-rimmed triangles) were supplemented by literature data stated in Fig. 5. Concentrations of (a) $Na_2O + K_2O$, (b) CaO, (c) $Al_2O_3$, (d) $SiO_2$, (e) $Fe_2O_3$, (f) $TiO_2$, and (g) $P_2O_5$ plotted against wt% MgO. (h) Molar Na/K-ratio vs. wt% MgO. All data represent original contents not renormalized to a volatile-free composition. For comparison, the compositions of the Kaiserstuhl and Katzenbuckel phonolites are also shown.

in phonolites exhibits variable and increased proportions of Na pyroxenes (7–70%) and up to 27% Tschermak's pyroxene at the expense of the quadrilateral components. Clinopyroxene in the groundmass of phonolites resembles clinopyroxene in (nepheline) syenites and is on average even more dominated by Na end-members (up to 80%) at lower tschermakitic components.

While diopsidic clinopyroxene in the melilitites–nephelinites contains a maximum of 25% hedenbergite component, the proportion in the crystal rims of the ijolite can increase up to 51%, with the aegirine component reaching up to 21% (Fig. 9b). The trend for clinopyroxene in the phonolites and (nepheline) syenites is evolving more strongly towards aegirine (8–81%) at hedenbergite components of 20–45%, although some pyroxene crystals show a lower hedenbergite content (5–20%) deviating from the general trend.

In the primitive rocks and the ijolitic patches, the Al content reaches up to 0.6 apfu and increases with decreasing Mg contents that range

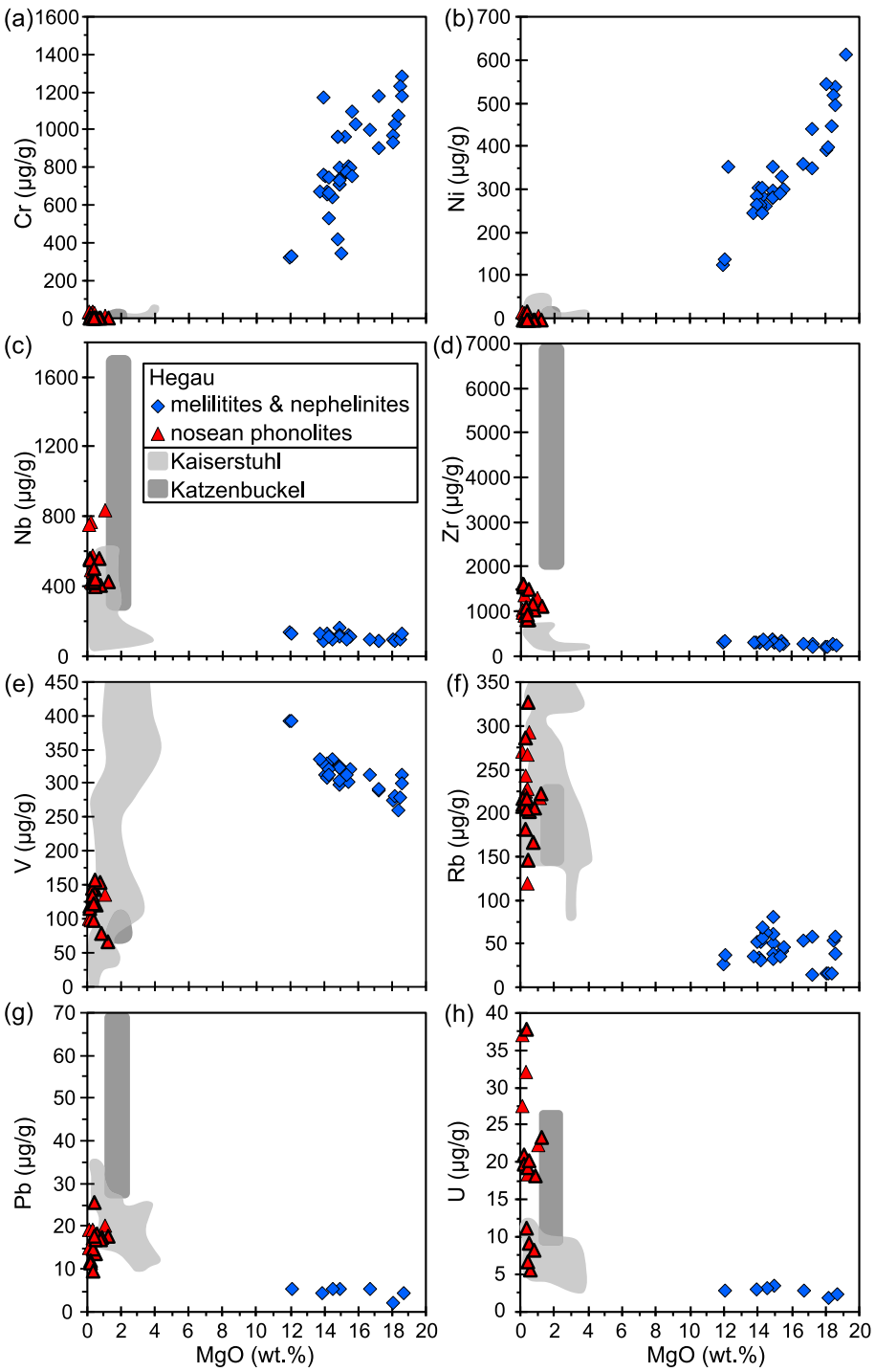


**Fig. 7.** Whole-rock trace element composition of the igneous Hegau rocks. 12 new analyses (black-rimmed triangles) were supplemented by literature data stated in Fig. 5. Concentrations (in µg/g) of (a) Cr, (b) Ni, (c) Nb, (d) Zr, (e) V, (f) Rb, (g) Pb, and (h) U plotted against wt% MgO. For comparison, the compositions of the Kaiserstuhl and Katzenbuckel phonolites are also shown.

from 0.52 to 0.88 apfu (Fig. 9c). Clinopyroxene rims in ijolite deviate from this trend and exhibit remarkably low Al (<0.05 apfu) and Mg concentrations (0.28–0.58 apfu). Clinopyroxene in the phonolites and (nepheline) syenites has even lower Mg contents (0.03–0.58 apfu), with the Al content (0.02–0.39 apfu) varying at Mg concentrations above 0.45 apfu but decreasing continuously at lower Mg contents. The same is observed for the Ti content (Fig. 9d), which is generally lower in the clinopyroxene rims of ijolite (0.04–0.08 apfu) and in the clinopyroxene of phonolites and (nepheline) syenites (<0.08 apfu) compared to that in the melilitites–nephelinites and to the macrocryst cores in the ijolite (<0.22 apfu). Usually, Zr does not exceed 1500 ppm; only in groundmass pyroxenes in phonolites, and in (nepheline) syenites Zr reach up to 6000 ppm (Fig. 9e).

### 4.3.2. *Alkali feldspar*

Alkali feldspar macrocrysts and microcrysts in the phonolites show no compositional differences and are $Or_{60-85}Ab_{15-40}$ with up to 8% celsian (Ba component) and variations within macrocrysts expressed in concentric zoning (Fig. 10a). The anorthite component (<0.4%; Fig. 10a) and Sr contents (2300 ppm) are very low. Alkali feldspar in the

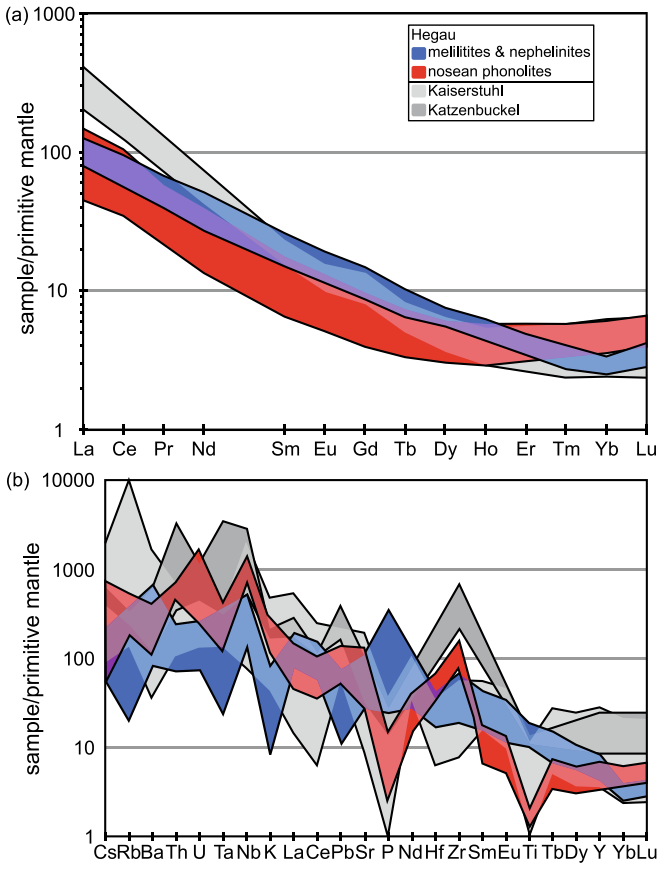


**Fig. 8.** Primitive mantle-normalized (a) REE pattern and (b) incompatible element pattern of the igneous Hegau rocks (normalization values from Palme and O'Neill, 2014); elements sorted by increasing mantle compatibility. Analyses are from the literature stated in Fig. 5. For comparison, the compositions of the Kaiserstuhl and Katzenbuckel phonolites are also shown.

(nepheline) syenites largely resembles this composition with few crystals reaching $Or_{93}$.

#### 4.3.3. Sodalite-group minerals

Haüyne-nosean-sodalite$_{ss}$ in melilitites–nephelinites is dominated by haüyne with a sodalite content of 15–20%, while those in the phonolites comprise two populations: (1) large macrocrysts with irregularly shaped deep blue S-rich, Cl-bearing unaltered domains ($Nsn_{48-65}Hyn_{28-45}Sdl_{6-10}$) and altered colourless to light glaucous domains ($Nsn_{89-100}Hyn_{0-11}Sdl_{0-1}$) and (2) smaller relatively homogeneous crystals exclusively having the latter composition (Figs. 3a, b & 10b). Further, haüyne-nosean-sodalite$_{ss}$ in the primitive rocks contains significant amounts of Ca and minor K, substituting 20–35% and ~ 10% of the Na, respectively. In contrast, a maximum of 4% of the Na in the S-rich, Cl-bearing domains and 21–37% in the altered domains in the macrocrysts of the phonolites are replaced by K, while Ca is almost completely absent (Fig. 10c).

#### 4.3.4. Oxyspinel

Skeletal oxyspinel crystals in the ijolitic patches are magnetite-ulvöspinel$_{ss}$ covering the same compositional range as in the melilititic–nephelinitic host rocks; exsolution lamellae in the skeletal crystals are Fe-rich ilmenite (Supplementary data, Fig. A2a). Mn (0.03–0.06 apfu), Zn (300–800 ppm), and V contents (2300–6000 ppm) largely correspond to the contents in most evolved oxyspinel of the primitive rocks and are comparatively high (Supplementary data, Fig. A2b-d). Oxyspinel is almost absent in the nosean phonolites.

#### 4.3.5. Perovskite

Skeletal perovskite in the ijolitic patches is generally more enriched in various trace elements than accessory perovskite in the melilititic–nephelinitic host rocks. However, the initial point of the mineral chemical evolution of the skeletal perovskite is always in the compositional range of the perovskite in the host rocks (Figs. 11a & b). Nb reaches up to 0.10 apfu and correlates positively with Ta (<3000 ppm; Fig. 11c) and Sr increases up to 0.05 apfu, correlating negatively with Ti (Fig. 11d). In perovskite in the ijolite, Fe (~0.01–0.03 apfu) decreases with advancing crystallization (Fig. 11e). Th (<6000 ppm) correlates positively with the REEs (<0.05 apfu), with the accessory perovskite in the melilitites–nephelinites sharing the same compositional range as the skeletal perovskite in the ijolite (Fig. 11f).

#### 4.3.6. Titanite

Titanite in the phonolites contains up to 0.04 apfu Zr, 9300 ppm LREE+Y, 0.06 apfu Nb, and 0.08–0.12 apfu Al + Fe (Supplementary Data, Fig. A3). Differences in the contents of these elements cause irregular to concentric zoning in the crystals, but without a distinct core-rim trend (Supplementary Data, Fig. A3c).

#### 4.3.7. Apatite

Apatite in melilitites–nephelinites and ijolite is fluorapatite, with a subordinate hydroxyapatite component and the chlorapatite component reaching 1–13%. Apatite in the phonolites varies between fluorapatite (24–89%) and hydroxyapatite (11–74%), the chlorapatite component being <2% (Fig. 12a). Apatite in the (nepheline) syenites is fluorapatite-hydroxyapatite$_{ss}$ lacking any detectable Cl. There are no significant differences between apatite in the different rocks regarding Na, Sr, Ba, and REEs (Fig. 12b).

## 5. Discussion

In the following, the genetic relationships between primitive olivine melilitites and melilite-bearing olivine nephelinites, rare ijolitic patches therein, (nepheline) syenite enclaves, and evolved nosean phonolites will be discussed and a comprehensive model for the magmatic evolution of the Hegau region will be presented.

### 5.1. Rare ijolite patches in melilititic–nephelinitic rocks: Evidence for rapid in-situ differentiation

In-situ differentiation in primitive olivine melilitites and melilite-bearing olivine nephelinites from Hohenstoffeln and Hohenhewen (Fig. 1b) is implied by rare coarse-grained and irregularly shaped ijolitic patches (Figs. 2c-g). Their geochemical composition is more evolved than that of the volcanic host as the contents of MgO, alkalis, $Al_2O_3$, and $Fe_2O_3$ fall between those of the melilitites–nephelinites and the nosean phonolites. Other compounds are slightly lower (e.g., $SiO_2$) or slightly higher (e.g., CaO, $TiO_2$, $P_2O_5$) than in the primitive rocks and do not fall on a linear trajectory between primitive and evolved rock suite (Fig. 6). This is reflected by the lack of olivine in the ijolitic patches, while clinopyroxene, nepheline, titanomagnetite, perovskite, and apatite are abundant (Figs. 2e-h). The crystallization trend of clinopyroxene evolves from diopsidic cores, which resemble the composition in the host rock, to aegirine- and hedenbergite-rich rims with similar Al and Ti contents as observed in phonolites and nepheline syenites (Fig. 9). Abundant skeletal perovskite and magnetite indicate rapid growth and a high degree of supersaturation of corresponding elements in the trapped residues due to fast undercooling (Figs. 2d, g & h; Gornitz, 1981). Compared to the composition in the host rock, perovskite shows continuous enrichment of Nb, Ta, Na, Sr, Th, and REE (Fig. 11), apatite is Cl- and $H_2O$-rich (Fig. 12), and magnetite is Mn- and V-rich (Supplementary data, Fig. A2), which indicates relative enrichment of these elements in the residual melt pockets (Fig. 2c). An interpretation of such in-situ fractionation as missing link between melilitites–nephelinites

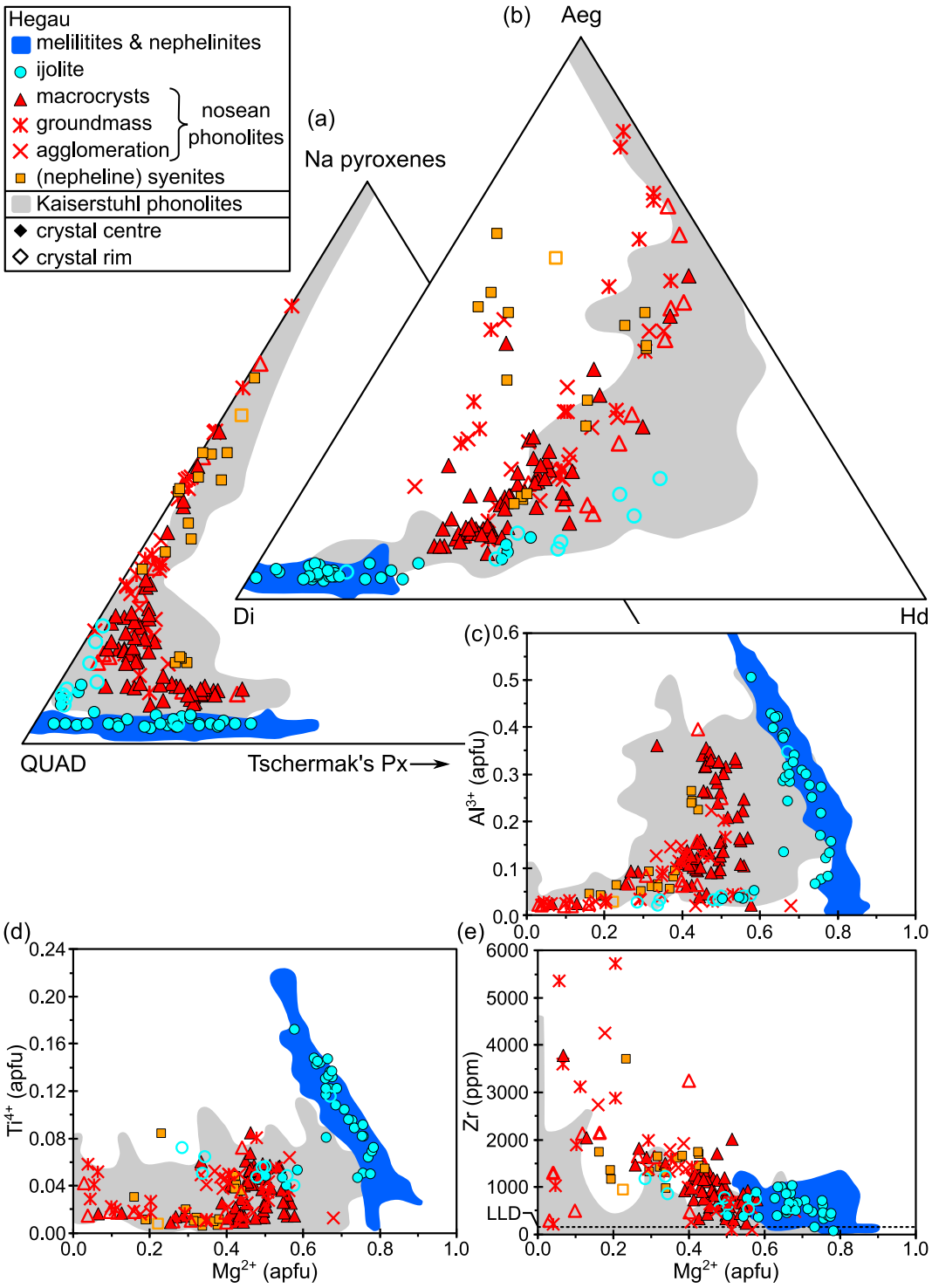


**Fig. 9.** Clinopyroxene composition in the igneous Hegau rocks. Data of this work supplemented by Binder et al. (in press). For comparison, the composition of clinopyroxene in the Kaiserstuhl phonolites is also shown (Braunger et al., 2018). (a) Triangular plot showing the distribution among the quadrilateral end-members (QUAD), Tschermak's clinopyroxenes ($CaXXSiO_6$ with X = Al, $Fe^{3+}$, Cr, Ti), and Na pyroxenes (aegirine – $NaFe^{3+}Si_2O_6$, Ti aegirine – $NaFe^{2+}_{0.5}Ti_{0.5}Si_2O_6$, jadeite – $NaAlSi_2O_6$). (b) Triangular plot showing the distribution among the end-members diopside (Di), aegirine (Aeg), and hedenbergite (Hd) normalized to 100%. $Mg^{2+}$ vs. (c) $Al^{3+}$, (d) $Ti^{4+}$, and (e) Zr. apfu – atoms per formula unit; LLD – lower limit of detection; ppm – parts per million.

and nosean phonolites is possible, although an expected increase in $SiO_2$ content and alkali feldspar saturation required for the evolution towards phonolites or nepheline syenites is not observed. It is suggested that in-situ crystallization under close-to-equilibrium conditions without sufficient removal of solids (i.e., lack of fractionation) and rapid cooling of the rocks prevented more extensive differentiation towards $SiO_2$-rich and CaO-, $TiO_2$-, $P_2O_5$-poor phonolitic compositions, a shallow fractionation trend which is often observed in plutonic rocks (e.g., in the Fen complex, Norway; Andersen, 1988).

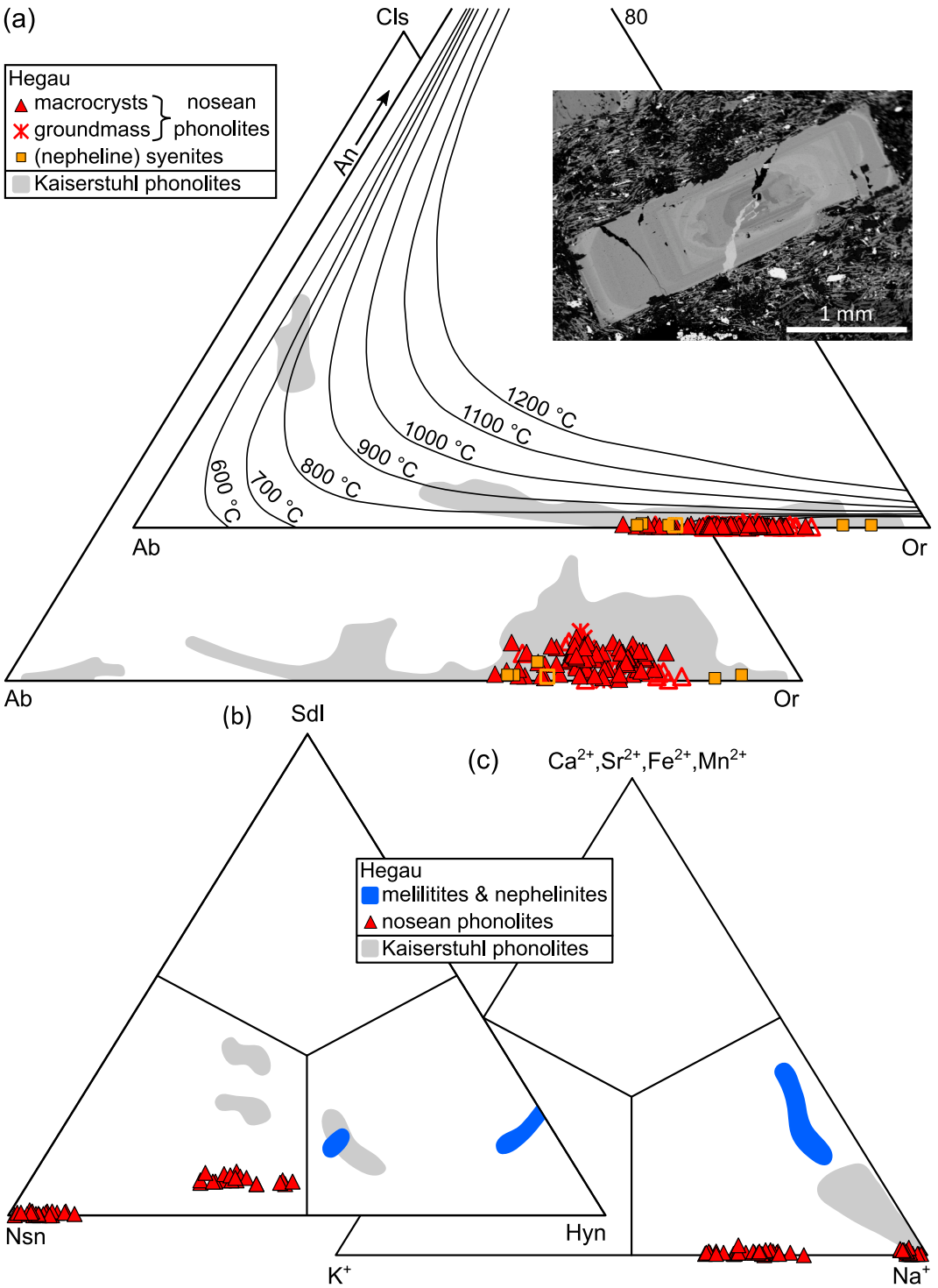


**Fig. 10.** Composition of feldspar and sodalite-group minerals in the igneous Hegau rocks. Data of this work supplemented by Binder et al. (in press). For comparison, the composition of feldspar and haüyne-nosean-sodalite$_{ss}$ in the Kaiserstuhl phonolites is also shown (Braunger et al., 2018). (a) Concentric compositional zoning of an alkali feldspar macrocryst in a nosean phonolite (Gönnersbohl) and triangular diagrams showing the distribution among the feldspar end-members celsian (Cls; Ba[$Al_2Si_2O_8$]), albite (Ab; Na[$AlSi_3O_8$]), and orthoclase (Or; K[$AlSi_3O_8$]) normalized to 100% and anorthite (An; Ca[$Al_2Si_2O_8$]), albite, and orthoclase normalized to 100%. Isotherms according to Fuhrman and Lindsley (1988). Triangular diagrams showing (b) the end-member composition of sodalite-group minerals based on the ratio between 2 $SO_4^{2-}$, $SO_4^{2-}$, and 2 $Cl^-$, with sodalite – $Na_6[Al_6Si_6O_{24}]Cl_2$ (Sdl), haüyne – $(Na,K)_6Ca_2[Al_6Si_6O_{24}](SO_4)_2$ (Hyn), and nosean – $Na_6[Al_6Si_6O_{24}]SO_4$ (Nsn), and (c) the molar K-Na-Ca,Sr,Fe,Mn distribution.

### *5.2. Nosean phonolites: products of fractional crystallization of melilititic–nephelinitic melts*

Primitive melilitites–nephelinites and evolved phonolites show overlapping age ranges (12–9 Ma and 14–11 Ma, respectively), but phonolitic volcanism started earlier and the existence of evolved rocks in the crust at the time of eruption of the primitive magmas is indicated by the entrained coarse-grained (nepheline) syenitic enclaves (Fig. 4a). These can be interpreted as cumulate rocks with alkali feldspar ± aegirine-augite as dominant cumulus crystals and variable amounts of

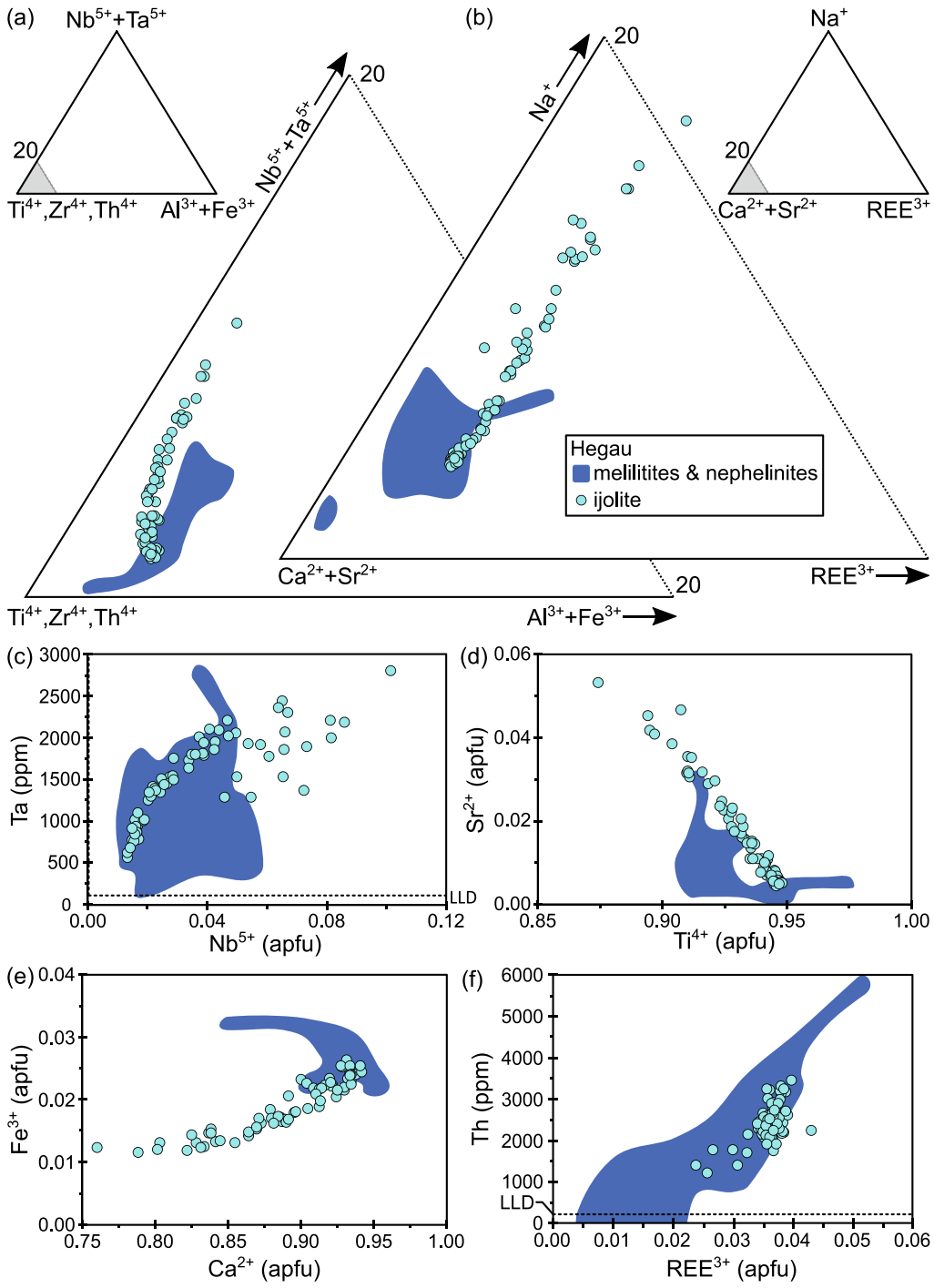


**Fig. 11.** Perovskite composition in the igneous Hegau rocks. Data of this work supplemented by Binder et al. (in press). Triangular diagrams showing (a) the molar Nb + Ta-Ti + Zr + Th-Al + $Fe^{3+}$ and (b) the Na-REE-Ca + Sr distribution normalized to 100%. (c) $Nb^{5+}$ vs. Ta, (d) $Ti^{4+}$ vs. $Sr^{2+}$, (e) $Ca^{2+}$ vs. $Fe^{3+}$, and (f) $REE^{3+}$ vs. Th. apfu – atoms per formula unit; LLD – lower limit of detection; ppm – parts per million.

nepheline, aegirine-augite, alkali feldspar, dark mica, and little carbonate representing the intercumulus melt (Figs. 4b-g). The variable proportions of nepheline and clinopyroxene, partly within the same enclave (Fig. 4b), indicate a layered arrangement of mesocratic and leucocratic lithologies and point to an evolving and convecting magma chamber that may have experienced repeated magma replenishment.

Since all recorded enclaves mirror an already highly fractionated and thus $SiO_2$- and alkali-enriched magma composition, the question remains as to the primary magma composition from which the nosean phonolites evolved by differentiation, and whether this could be the same magma composition represented by the primitive melilitites–nephelinites. In this case, the older phonolitic volcanoes would have erupted only after significant magmatic differentiation in the crust, while the mostly younger melilititic–nephelinitic magmas would have been transported "directly" from mantle to surface. The evolution of clinopyroxene composition (Fig. 9) and the presence of sodalite group minerals (Fig. 10) in both the melilitites–nephelinites and phonolites support this assumption. The differences between primitive and evolved rocks in terms of clinopyroxene composition are consistent with the evolution of the whole-rock composition towards very low MgO and

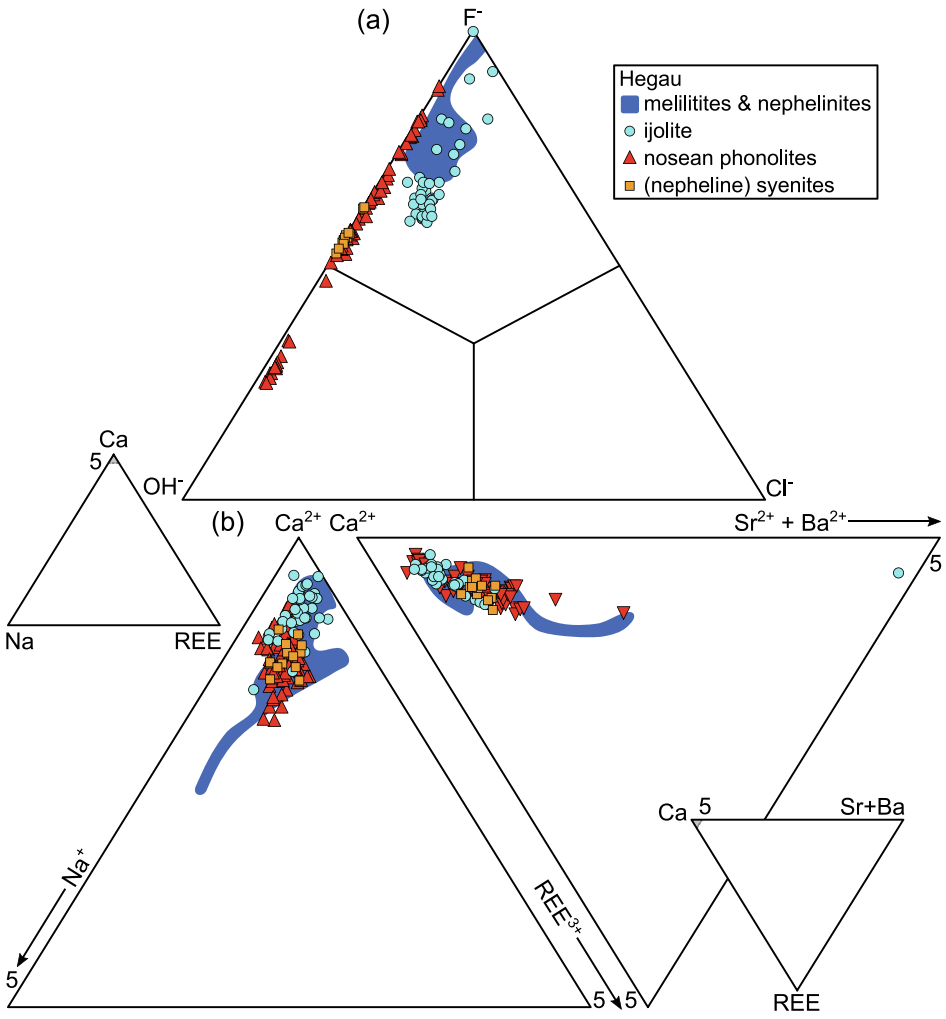


**Fig. 12.** Apatite composition in the igneous Hegau rocks. Data of this work supplemented by Binder et al. (in press). (a) Triangular classification diagram based on the anion position ($OH^-$, $F^-$, $Cl^-$). (b) Triangular diagrams showing the molar Ca-Na-REE and Ca-Sr + Ba-REE distribution each normalized to 100%.

CaO, and low $Fe_2O_3^{tot}$ contents (Figs. 6b & e). The marked decrease in CaO content and increase in $K_2O$ content relative to the primitive rocks is also evident in the composition of the sodalite-group minerals: in the phonolites, these minerals lack Ca, but partially contain K, whereas for those in the melilitites–nephelinites, a high Ca content and hardly any K is observed (Fig. 10c). Higher $Na_2O$, $Al_2O_3$, and $SiO_2$ contents in phonolites (Figs. 5 & 6c) are reflected by abundant nepheline and alkali feldspar and the presence of titanite instead of perovskite, as it was observed in the primitive rocks including their ijolitic patches.

The primitive mantle-normalized REE patterns show a continuous decrease in enrichment towards the HREE, which for the primitive rocks can be explained by residual garnet in the mantle source that fractionates LREE from HREE (e.g., Kolb et al., 2012; Ulrych et al., 2011). The phonolites show a comparable enrichment factor for the REE, but with a marked trough of the MREE and higher contents of HREE relative to the primitive rocks (Fig. 8a). This can be explained by titanite fractionation, a mineral that enriches MREE over LREE and HREE (Prowatke and Klemme, 2005), and is supported by a remarkable negative Ti anomaly in the primitive mantle-normalized trace element pattern for phonolites (Fig. 8b), and by low Ca and Ti contents in the whole rock (Figs. 6b & f). Likewise, the fractionation of Zr from Hf (Zr/Hf = 78–103) and Nb from Ta (Nb/Ta = 38–82) in the phonolites (Fig. 8b; Supplementary data, File 1) can be attributed to titanite fractionation, as this mineral is more compatible for the heavy than the lighter geochemical twins (e.g., Berger et al., 2014). In contrast, the Zr/Hf ratios in the primitive melilitites–nephelinites are lower and relatively constant (38–44; cf. primitive mantle: ~34), whereas the Nb/Ta ratios vary already considerably (18–42; cf. primitive mantle: ~14), which may be attributed to different amounts of residual phlogopite (Green et al., 2000) or prior carbonate metasomatism in their mantle source (e.g., Pfänder et al., 2012).

The general lack of strong REE enrichment in the phonolites relative to the melilitites–nephelinites (Fig. 8a) is caused by apatite and possibly pyrochlore fractionation, in accordance with a striking P trough in the trace element pattern of the phonolites (Fig. 8b), and with low Ca contents in the whole rock. Abundant apatite, titanite, and accessory pyrochlore (Figs. 4h-k) in the entrained (nepheline) syenites corroborates fractionation of these minerals to generate the residual phonolitic melt. The remaining trace element patterns reflect relative enrichment of certain incompatible elements (e.g., Cs, Th, U, Ta, K, Nb, Hf, and Zr) in the evolved melt manifested by the accessories zircon, titanite, and pyrochlore, and elevated contents of Zr in clinopyroxene (Fig. 9e) as well as orthoclase-rich feldspar in the phonolites (Fig. 10a). The partly high Ba concentrations in alkali feldspar of the groundmass and in zoned phenocrysts (Fig. 10a) can be explained by high Ba contents in the parental melt (Fig. 8b) and further enrichment during fractionation, as is typical of nephelinite-derived phonolites (Le Bas, 1987). The lack of Cl in apatite in the nosean phonolites compared to ijolite and the primitive rocks (Fig. 12) may be due to the presence of abundant haüyne-nosean-sodalite$_{ss}$ in the evolved rocks incorporating all the Cl.

The slightly positive Pb anomaly compared to the strongly negative one in the primitive rocks (Fig. 8b), low Ce/Pb and strongly varying Nb/U ratios (Supplementary data, Fig. A4) could indicate assimilation of continental crust, as this would lower these ratios in mantle-derived magmas (e.g., Jung et al., 2012). In the CEVP and elsewhere, the formation of phonolites has been attributed mainly to fractional crystallization with subordinate to negligible crustal assimilation (Berger et al., 2009; Bourdon et al., 1994; Ulrych et al., 2003; Vaněčková et al., 1993; Wörner and Schmincke, 1984) or to significant and various amounts of crustal assimilation of e.g., mica schists, granites, paragneisses, metapelites, and mafic granulites (Jung et al., 2013; Kolb et al., 2012; Panina et al., 2000; Schleicher et al., 1990; Schmitt et al., 2017). However, verification and quantification of assimilation in the case of the Hegau phonolites would require isotopic data.

### 5.3. A thermodynamic modelling approach

To test the hypothesis that phonolites originate from fractional crystallization of olivine melilitites and melilite-bearing olivine nephelinites, the MELTS software package was used. Temperatures of up to 1350 °C for partial melting of the source lithology of the primitive melilitites–nephelinites of the Hegau region have been inferred by Binder et al. (in press) and are consistent with those for similar rocks from the CEVP (e.g., Jung et al., 2012; Mayer et al., 2013). However,

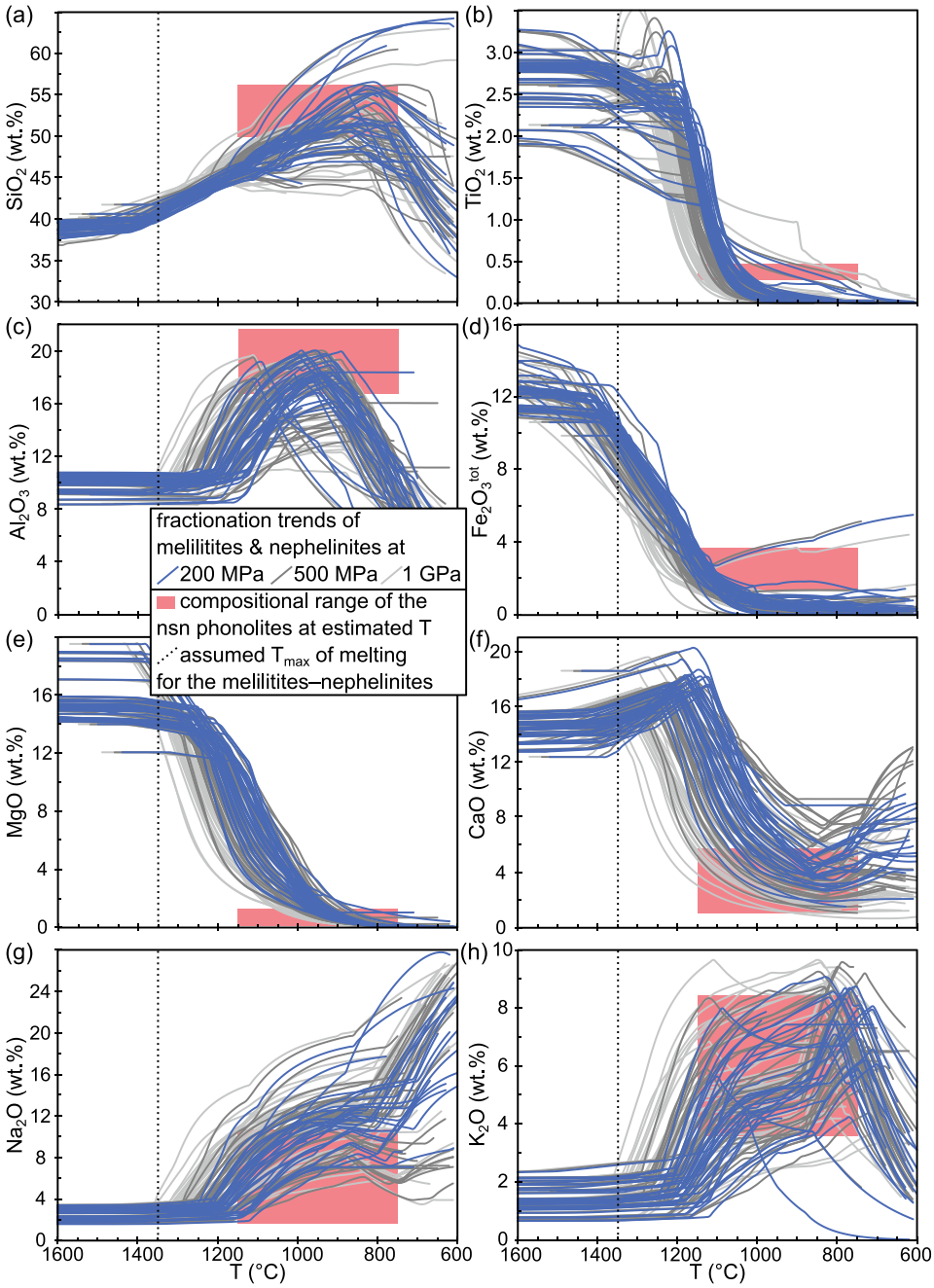


**Fig. 13.** Results of fractional crystallization modelling of melilititic–nephelinitic Hegau magmas at 200, 500 and 1000 MPa using MELTS (Ghiorso and Sack, 1995). The whole-rock compositions of the primitive rocks served as input data. For all major oxides, including (a) $SiO_2$, (b) $TiO_2$, (c) $Al_2O_3$, (d) $Fe_2O_3^{tot}$, (e) MgO, (f) CaO, (g) $Na_2O$, and (h) $K_2O$ (each in wt%), phonolitic compositions can be realized by magmatic differentiation without significant crustal assimilation at temperatures of 750–1150 °C. The light red rectangles show the range of the whole-rock composition of the Hegau phonolites. (For interpretation of the references to colour in this figure legend, the reader is referred to the web version of this article.)

actual modelling was performed and depicted with higher starting temperatures to identify and avoid potential artifacts (discussed below). Residual melt fractions of >95 mass% and thus no significant changes in melt composition are predicted for most model curves until plausible liquidus temperatures for melilitites–nephelinites are reached (Figs. 13 & 14). Therefore, the used model parameters and most whole-rock analyses of the melilitites–nephelinites are considered suitable for testing fractional crystallization towards phonolites. A corresponding composition should be achieved at realistic temperatures and with a quantifiable residual melt fraction to propose fractional crystallization of melilititic–nephelinitic magmas in a closed system without requiring significant assimilation. All the phonolites have porphyritic textures, which indicates continuous crystallization during cooling. Additionally, magma convection and replenishment events can result in cumulate remobilization and remelting and/or entrainment of cumulate crystals, resetting the melt towards less evolved compositions and rendering a wide temperature interval conceivable (e.g., Sliwinski et al., 2015; Wörner and Wright, 1984). Thus, different element contents would not necessarily reach the concentrations observed in the nosean phonolites at the same temperature.

For crustal pressures between 200 and 1000 MPa, the range of whole-rock compositions of the phonolites can be reproduced (except for Mn and P) at temperatures of 750–1150 °C (Figs. 13 & 14; Supplementary data, Fig. A1), with upper crustal pressures (i.e., 200 MPa)

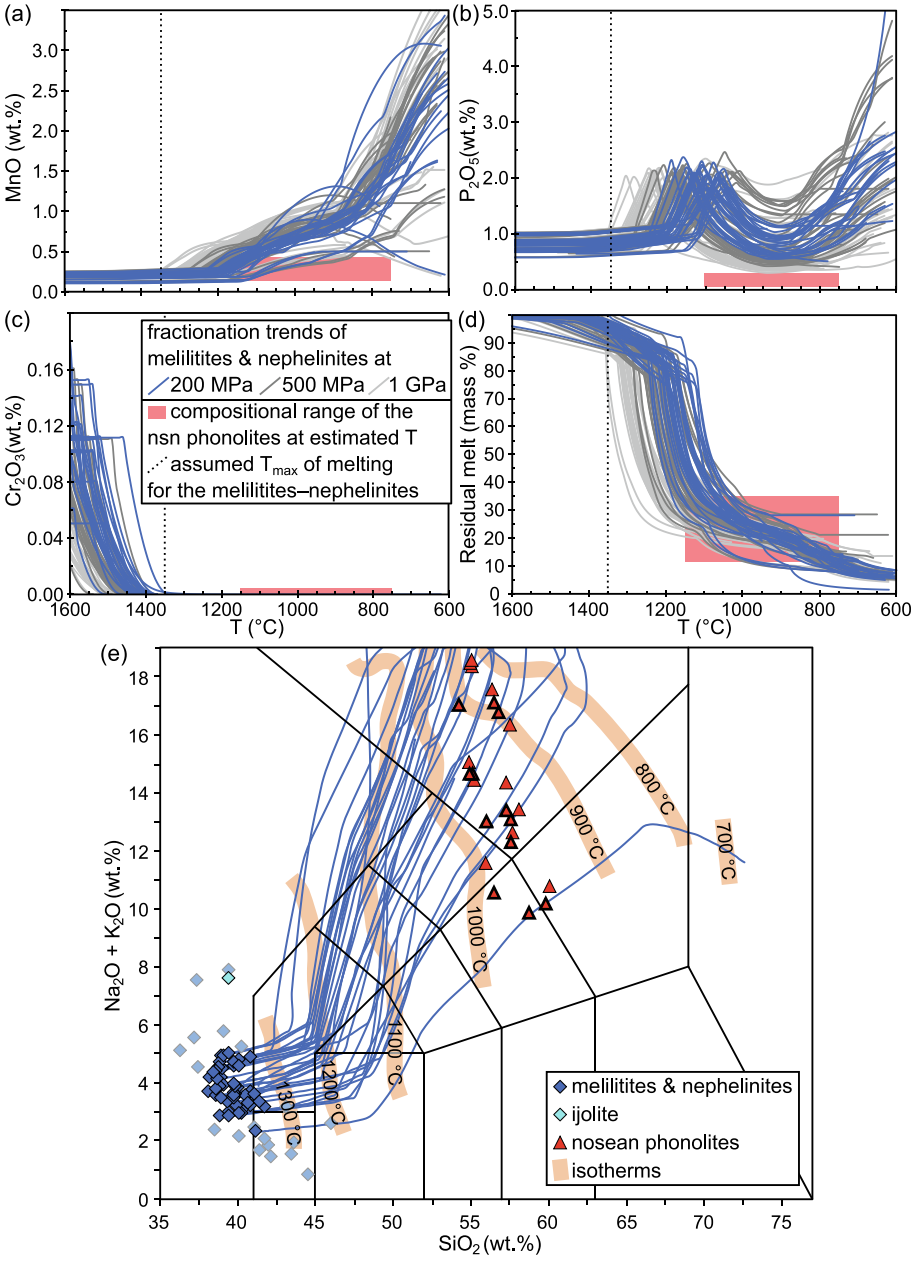


**Fig. 14.** Results of fractional crystallization modelling of melilititic–nephelinitic Hegau magmas at 200, 500 and 1000 MPa using MELTS (Ghiorso and Sack, 1995). The whole-rock compositions of the primitive rocks served as input data. (a) MnO, (b) $P_2O_5$, and (c) $Cr_2O_3$ (each in wt%). (d) Melt residues of ~12–35 mass% of the initial magma are responsible for most calculated phonolite compositions, regardless of formation pressure. (e) TAS diagram showing compositions of the volcanic Hegau rocks. 12 new analyses (black-rimmed triangles) were supplemented by literature data stated in Fig. 5. The trajectories show the melt evolution of melilititic–nephelinitic magmas predicted by MELTS modelling with whole-rock compositions of the primitive rocks as input data. For compositions from which no graphs emanate (pale blue squares), fractionation modelling was not successful. (For interpretation of the references to colour in this figure legend, the reader is referred to the web version of this article.)

tending to achieve the best-fit compositions. Geothermometric results for fractional crystallization towards phonolitic composition elsewhere reveal a similarly wide temperature range. Monchiquite- and tephrite-derived KVC phonolites started crystallizing at ~880–960 °C (Braunger et al., 2018) or at ~1040–1060 °C (Panina et al., 2000), while for the nephelinite-derived Katzenbuckel phonolite ~780–880 °C were estimated (Mann et al., 2006). The basanite-derived Laacher See mafic phonolite (East Eifel) reveals melt temperatures of ~860–1060 °C and the more evolved felsic one 720–860 °C (Berndt et al., 2001; Bourdon et al., 1994; Ginibre et al., 2004; Schmitt et al., 2010; Wörner and Wright, 1984). However, for sanidine and plagioclase (~950–1125 °C) and haüyne and apatite phenocrysts (1120–1180 °C) in the Upper Laacher See Tephra even higher crystallization temperatures were postulated (Sharygin et al., 2005). Alkaline rocks from Tenerife underwent a two-stage evolution from basanites via phonotephrites to phonolites with main crystallization intervals at ~1150–1110 °C and ~925–875 °C (Sliwinski et al., 2015).

No thermodynamic data for the Mn clinopyroxene end-member johannsenite and for fluorapatite are implemented in the MELTS database, which explains observed misfits concerning MnO and $P_2O_5$ (Figs. 14a & b). Further, the modelled Cr content drops by fractionation of oxyspinel well before the assumed melting temperatures for the primitive rocks are reached (Fig. 14c). This may be due to the lack of a Cr-bearing pyroxene in the MELTS database and/or excessively high Cr contents in the rocks because of Cr-rich oxyspinel and Cr-diopside xenocrysts (see Binder et al., in press). For a few whole-rock compositions of the primitive rocks with particularly low or high alkali contents, the modelling attempt resulted in an abortion of the computation, so that no differentiation path could be determined (pale blue squares in Fig. 14e). This may indicate that those whole-rock compositions do not represent primary melt compositions due to high xenocryst and antecryst loads, hydrothermal alteration, or low-temperature weathering.

Overall, modelling implies that, depending on the assumed initial composition and depth of the magma chamber, ~12–35 mass% of the initial melilititic–nephelinitic melt remains as residue when phonolitic compositions are reached (Fig. 14d). This agrees with estimates for phonolite evolution from Laacher See, for which 30 mass% derivative melt of a basanitic magma were calculated (Wörner and Schmincke, 1984). During melt evolution, $SiO_2$ and $Na_2O + K_2O$ enrichment is predicted, resulting in differentiation trajectories via basanites/tephrites ±(trachy)basalts, phonotephrites and tephriphonolites ±alkali-rich foidites to phonolites (blue curves in Fig. 14e). In particular, the lower alkali melilititic–nephelinitic magmas undergo a melt evolution resulting in the observed $SiO_2$ and alkali contents of the nosean phonolites at ~850–1000 °C (Fig. 14e).

Early fractionation of olivine (4–10%) and oxyspinel (11–19%) is predicted for most initial compositions (Figs. 15a & b). However, up to 3 mass% oxyspinel crystallization postulated at >1350 °C is likely caused by entrainment of mantle xenocrysts, leading to such modelling artifacts. These are only small quantities, so the effect should be negligible for the overall modelling, especially since this very early alleged fractionation partially corrects excessive Cr and Mg contents in whole-rock compositions towards actual melt compositions. Subsequently, extensive clinopyroxene fractionation (42–57%) is predicted (Fig. 15c), consistent with clinopyroxene in the mesocratic (nepheline) syenite enclaves (Table 2; Figs. 4f & g). Considering variable amounts of macrocrysts, but also microcrysts of clinopyroxene in the phonolites (<10% in total; Table 2; Figs. 3a-d), it can be assumed that its crystallization occurred over a long time and temperature interval and that fractionation and separation was not yet completed at the time of ascent of the phonolitic melt. This suggests temperatures of >900 °C at the time of melt extraction as clinopyroxene formation stops at lower temperatures (Fig. 15c).

Mica fractionation (<3%) is forecast from 1050 to 800 °C (Fig. 15d), supported by the mineralogy of (nepheline) syenites and phonolites (Table 2; Figs. 4e & f). The onset of feldspathoid crystallization (~3–9%), with two exceptions, occurs below 1000 °C, that of feldspar (mostly ~2–8%) below ~950 °C, continuing in each case until complete solidification of the proposed melts (Figs. 15e & f). Since the (nepheline) syenites also contain both phases as major minerals, formation of these rocks must have continued until cooling to at least 900 °C, more likely 800 °C. This correlates well with the crystallization of the phonolites as volcanic counterparts, and feldspar geothermometry, yielding temperatures below 800 °C (Fig. 10a).

It must be considered that the thermodynamic database of MELTS does not contain sodalite-group minerals, so nepheline is possibly overestimated and depending on the Na/K ratio and $aSiO_2$, additional feldspathoids (leucite, kalsilite) are erroneously predicted. However, the total amount of feldspathoids formed is plausible, since their average stoichiometry is similar with respect to the Al-Si-alkali ratio, and they form under comparable physicochemical conditions. The onset of garnet crystallization, which occurs in neither the nosean phonolites nor the (nepheline) syenites, is predicted at 750–700 °C (Fig. 15g), most likely representing sub-solidus temperatures for the rocks (e.g., Braunger et al., 2018; Mann et al., 2006). However, MELTS only includes the pyralspite solid solution series and the grossular end-member, but not andradite, so interpretations regarding garnet formation must be questioned. Further, 1–2% apatite fractionation may have been slightly underestimated (Fig. 15h) as the software considers only hydroxyapatite, yet F-dominated apatite prevails in the primitive and evolved rocks (Fig. 12a).

In summary, we propose crystallization of the phonolites between 1050 and 750 °C from an evolved magma of initially melilititic–nephelinitic composition, resembling the geochemical characteristics of the primitive Hegau rocks. Fractional crystallization occurred mainly in the upper crust (~200 MPa) and formed (nepheline) syenitic cumulates at 1050–800 °C, fragments of which were entrained into the ascending phonolitic, melilititic–nephelinitic magmas, and into melts forming the mafic augite-hornblende-phlogopite tuffs, causing the contemporaneous and subsequent eruptions in the Hegau region. Fractionation of 11–19% oxyspinel, 4–10% olivine, 42–57% clinopyroxene, <3% mica, <9% feldspathoids, <8% feldspar in the order mentioned, and minor amounts of titanite and apatite (~2%) result in a phonolitic melt residue representing ~12–35 mass% of the initial melt. Given the lack of isotope data, crustal contamination (assimilation) during fractional crystallization cannot be ruled out, although the modelling results imply that it is not required to explain the observed phonolite compositions.

### 5.4. The Daly gap and implications for magma ascent and emplacement

Why did pronounced upper crustal differentiation processes in the central eastern Hegau region at ~15–11 Ma (ages of nepheline syenites and syenites) culminated in the emplacement of phonolite domes 14–11 Myr ago, whereas largely undifferentiated primitive melilititic–nephelinitic lavas were emplaced in the northern and western Hegau region during and after phonolitic activity from 12 to 9 Ma? We suggest that the compositional gap between primitive and evolved magmas is due to the largely separated crystallization and segregation of specific mineral phases and the thermodynamically and rheologically favoured timing of melt extraction. MELTS modelling shows that down to a temperature of ~1100–1050 °C, predominantly the mafic minerals oxyspinel, olivine, and clinopyroxene as well as small amounts of apatite crystallize from a fractionating primitive, initially melilitite- and nepheline-normative magma and consequently reduce the melt to ~30–50% of the bulk (Figs. 14d & 15a-c). The lack of entrained enclaves or individual crystals of such wehrlitic to olivine-pyroxenitic cumulates in the phonolites is probably the result of effective gravitational separation of these dense mafic cumulus minerals from the light intermediate to felsic residual melt or complete dissolution because of strong disequilibrium with the continuously evolving residual melt.

Clinopyroxene and apatite formation continued down to ~900 °C,

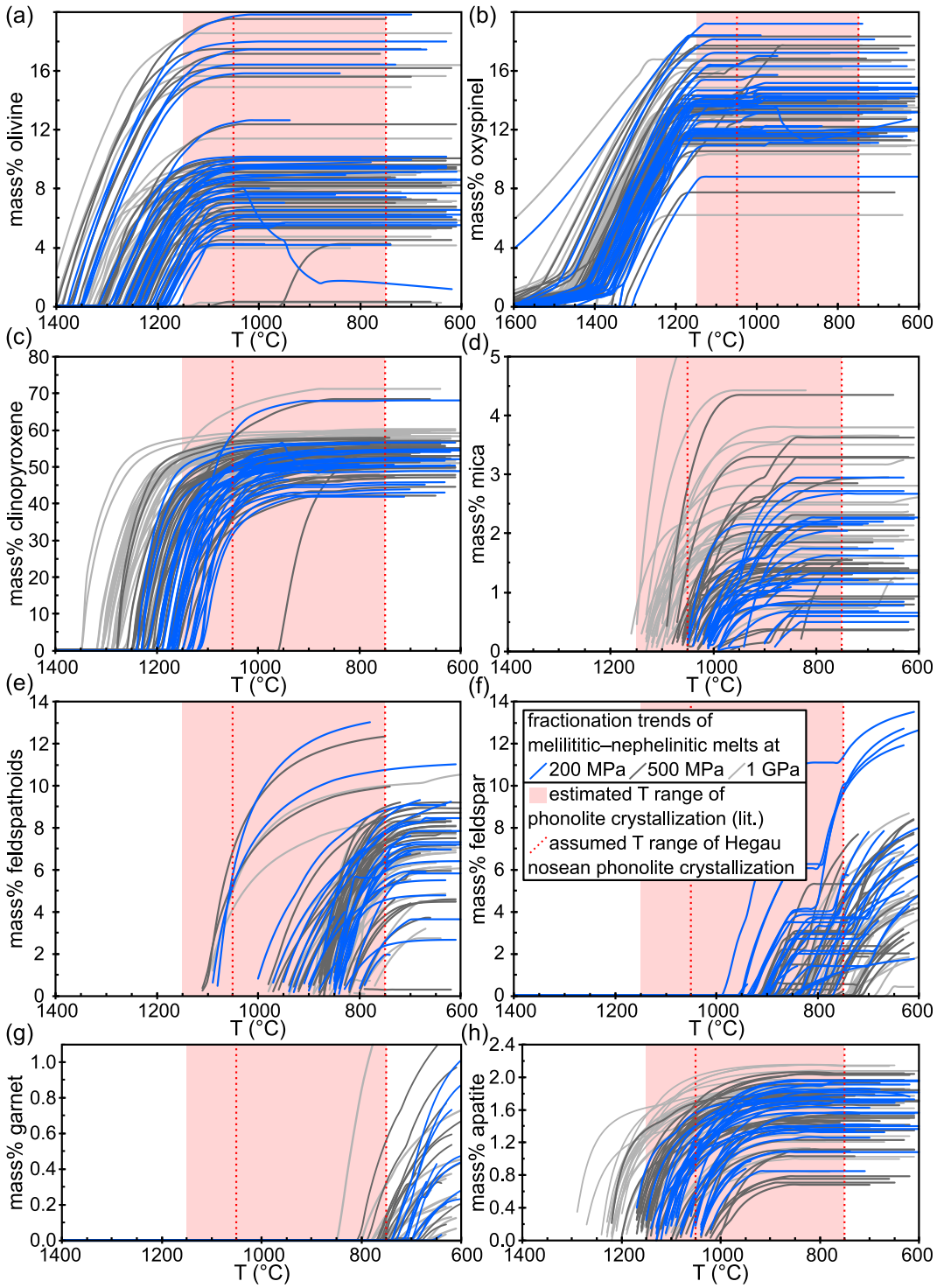


**Fig. 15.** Results of fractional crystallization modelling of melilititic–nephelinitic Hegau magmas at 200, 500 and 1000 MPa using MELTS (Ghiorso and Sack, 1995). The whole-rock compositions of the primitive rocks served as input data. Estimated fractionation of phases depending on temperature; (a) olivine, (b) oxyspinel, (c) clinopyroxene, (d) mica, (e) feldspathoids, (f) feldspar, (g) garnet, and (h) apatite (each in mass%).

while mica, feldspar, and feldspathoids started crystallizing between 1050 and 950 °C, proceeding until the phonolites solidified. This period of fractional crystallization is well recorded by the macrocryst load of the nosean phonolites and by the differently composed (nepheline) syenite cumulate enclaves (Table 2). They are characterized by a continuous evolution of mesocratic (nepheline) syenites with up to 30 vol% clinopyroxene and 5 vol% dark mica ± apatite, titanite, and zircon to leucocratic (nepheline) syenites with alkali feldspar and dark mica ± nepheline, carbonate, titanite, pyrochlore, zircon, thorite, and thorianite (Fig. 4). Possibly, magma replenishment of intermediate composition triggered the eruption of the phonolites with entrainment of cumulate fragments and crystals at a temperature > 900 °C when clinopyroxene and apatite still crystallized. Related models to explain compositional gaps in bimodal alkaline volcanism (Canary Islands, Ethiopian Rift) likewise include substantial temporal separation between the crystallization of mafic and felsic minerals and preferential magma mobilization

at specific times. This is explained by exceeding the intermediate differentiation stage within a narrow temperature interval with a respectively low crystallization rate (Peccerillo et al., 2003) or by optimal melt extraction from a crystal mush at intermediate crystallinity (i.e., 30–60% fractionation; Sliwinski et al., 2015). Accordingly, the latter is associated with favourable rheological conditions and released heat of crystallization, which lowers the crystallization rate, providing time for crystal-magma separation.

Moreover, variations of density and plasticity of different basement lithologies and deflection along the interface of low-angle thrust faults may have affected the buoyancy of mafic melts, protracting ascent and allowing differentiation of the magmas in some cases (e.g., Lusatian Volcanic field; Büchner et al., 2015). In the Eger Graben, primitive olivine melilitites and olivine nephelinites are associated with phases of compressional stress and occur mainly in the pre-rift and subordinately in the late-rift period, while more evolved rocks dominate in the *syn*-rift phase under extensional stresses (Ulrych et al., 2011). Accordingly, volcanic rocks coeval with compressive stresses are associated with major faults, whereas volcanism coinciding with extensional stress shows a much weaker structural control, which may hinder rapid ascent and protract differentiation. Similarly, Przybyla et al. (2018) suggest a phase of intense rifting, i.e., a discrete event of lithosphere stretching and/or disruption to have caused a short phase of felsic volcanism in the Siebengebirge near Bonn, whereas undifferentiated mafic lavas erupted over a longer period before and after (>8 Myr). They propose a magmatic plumbing system, which emptied from the top down over more evolved to more primitive lavas within <1 Myr.

Analogously, we propose a structurally controlled mechanism for differentiation, ascent, eruption, and emplacement of the Hegau magmas governed by the regional geodynamic evolution. The latest possible onset of upper crustal differentiation processes is documented by the oldest (nepheline) syenite ages (~15 Ma, Hohenstoffeln; Fig. 1; Binder et al., 2023) and extends over wide areas of the Hegau basement. This is evidenced by corresponding enclaves in numerous occurrences of volcanic rocks scattered throughout the region and consistent with remote sensing and GIS studies, indicating an extensive sub-surface, ring-shaped magmatic structure (Theilen-Willige, 2011). Pronounced uplift in the Vosges-Swabian arc, i.e., at the southern end of the South German Block including the Hegau region, reflected by a phase of intensified erosion in the Swabian Alb (Ring and Bolhar, 2020), may have triggered this magmatic activity. Uplift and erosion proceeded during late Miocene to early Pliocene shortening and provoked thin-skinned thrusting and folding in the Jura Mountains and Molasse basin (<12–10 Ma; Becker, 2000; von Hagke et al., 2012), overlapping with the age of the younger primitive volcanic rocks in the study area. Thus, intensified uplift and rifting may have firstly led to the development of larger upper crustal magma chambers and associated differentiation processes producing (nepheline) syenite cumulates and phonolitic melts. Subsequently, ongoing, progressive graben formation and disruption of the upper crust by emergence of local and/or (re) activation of deep-seated fault systems may have facilitated rapid magma ascent such that eruptions of melilititic–nephelinitic melts and mafic tuffs occurred without extensive fractionation. Obviously, this does not exclude a temporal overlap of the different manifestations of volcanism in the Hegau region, which can be explained by the spatial heterogeneity of the faulted crust.

## 6. Conclusions

Based on petrography, mineral chemistry, fractionation modelling, and previous U—Pb geochronology, the following model for the magmatic evolution in the Hegau region is proposed.

(1) The composition of evolved nosean phonolites (14–11 Ma) can be modelled by fractional crystallization of a melilititic–nephelinitic magma, whose composition resembles that of regional primitive olivine melilitites and melilite-bearing olivine nephelinites (12–9 Ma). Fractionation of 11–19% oxyspinel, 4–10% olivine, 42–57% clinopyroxene, <3% mica, <9% feldspathoids, <8% feldspar, and minor amounts of titanite and apatite results in phonolitic residues that represent ~12–35 mass% of the initial melt. The large compositional range of the nosean phonolites is explained by relatively small differences in potential parental melt compositions and variable degrees of fractionation. Crustal assimilation is not excluded but not essential to explain the mineralogical, mineral chemical, and geochemical features.

(2) The modelled compositions representing the observed phonolite compositions best were achieved for a pressure of 200 MPa, consistent with upper crustal formation conditions for phonolites in the CEVP and elsewhere. The predicted mineral assemblages agree largely with the petrography of the nosean phonolites and (nepheline) syenite cumulates, suggesting that the latter crystallized at temperatures of 1050–800 °C and that the phonolite melt was extracted at >900 °C.

(3) A temporal progression from evolved rocks that experienced prolonged differentiation in upper crustal magma chambers (nosean phonolites) towards near-primary, fast ascending primitive melts (melilititic–nephelinitic rocks) could explain the sequence of eruptions in the Hegau region. The onset of magmatism corresponds temporally with a regional phase of intensified erosion in response to pronounced uplift in the Vosges-Swabian arc. This may have firstly led to the development of larger upper crustal magma chambers and associated differentiation processes that produced (nepheline) syenite cumulates and phonolitic melts. Increased uplift and erosion during late Miocene to early Pliocene crustal shortening coincide with the age of the younger, but more primitive volcanic rocks. Thus, ongoing, progressive graben formation may have facilitated magma ascent such that eruptions of melilititic–nephelinitic melts and mafic tuffs occurred without extensive prior fractionation.

## Funding

This work was supported by the Deutsche Forschungsgemeinschaft (DFG) [grant MA 2563/19 & WA 3116/6]. The funding source was not involved in the study design, in the collection, analysis and interpretation of data, in the writing of the manuscript, and in the decision to submit the article for publication.

## Declaration of competing interest

Thomas Binder reports financial support was provided by Deutsche Forschungsgemeinschaft. If there are other authors, they declare that they have no known competing financial interests or personal relationships that could have appeared to influence the work reported in this paper.

## Data availability

The data underlying this article are available in the article and in its online supplementary data. Whole-rock geochemistry was supplemented by literature data from Alibert et al. (1983), Dunworth and Wilson (1998), Engelhardt and von Engelhardt and Weiskirchner (1961), Keller et al. (1990), Krause (1969), Krause and Weiskirchner (1981), Staesche (1995), Stock (1990), and Wimmenauer (1974).

## Acknowledgements

We are grateful to the Deutsche Forschungsgemeinschaft (DFG) for financial support for the acquisition of the electron probe microanalyzer [grant: INST 37/1026-1 FUGG]. We thank the Landesamt für Geologie,

Rohstoffe und Bergbau (LGRB, Freiburg im Breisgau) and Udo Neumann (University of Tübingen) for providing samples used in this study. Thanks also to Simone Schafflick and Philip Werner (University of Tübingen) for sample preparation. Moreover, we thank Elisabeth Eiche, Claudia Mößner, and Janine Wagner (LERA, KIT) for their support in the whole-rock analyses. We gratefully acknowledge the constructive reviews by Juliana Troch and an anonymous reviewer, as well as the handling by the co-editor-in-chief Greg Shellnutt.

## Appendix A. Supplementary data

Supplementary data to this article can be found online at https://doi.org/10.1016/j.lithos.2024.107565.

## References

Alibert, C., Michard, A., Albarède, F., 1983. The transition from alkali basalts to kimberlites: Isotope and trace element evidence from melilitites. Contrib. Mineral. Petrol. 82, 176–186.
Andersen, T., 1988. Evolution of peralkaline calcite carbonatite magma in the Fen complex, Southeast Norway. Lithos 22, 99–112.
Becker, A., 2000. The Jura Mountains — an active foreland fold-and-thrust belt? Tectonophysics 321, 381–406.
Berger, J., Ennih, N., Mercier, J.-C.C., Liégeois, J.-P., Demaiffe, D., 2009. The role of fractional crystallization and late-stage peralkaline melt segregation in the mineralogical evolution of Cenozoic nephelinites/phonolites from Saghro (SE Morocco). Mineral. Mag. 73, 59–82.
Berger, J., Ennih, N., Liégeois, J.-P., 2014. Extreme trace elements fractionation in Cenozoic nephelinites and phonolites from the Moroccan Anti-Atlas (Eastern Saghro). Lithos 210-211, 69–88.
Berndt, J., Holtz, F., Koepke, J., 2001. Experimental constraints on storage conditions in the chemically zoned phonolitic magma chamber of the Laacher See volcano. Contrib. Mineral. Petrol. 140, 469–486.
Binder, T., Marks, M., Walter, B.F., Wenzel, T., Markl, G., 2024. Two Distinct Metasomatized Mantle Sources Produced Two Groups of Alkaline $SiO_2$-undersaturated Rocks in the Southern Central European Volcanic Province. J. Petrol. in press.
Binder, T., Marks, M.A.W., Walter, B.F., Wenzel, T., Markl, G., Gerdes, A., Grimmer, J., Beranoaguirre, A., 2023. Two distinct age groups of melilitites, foidites, and basanites from the southern central European Volcanic Province reflect lithospheric heterogeneity. Int. J. Earth Sci. 112, 881–905.
Blusztajn, J., Hegner, E., 2002. Osmium isotopic systematics of melilitites from the Tertiary central European Volcanic Province in SW Germany. Chem. Geol. 189, 91–103.
Bourdon, B., Zindler, A., Wörner, G., 1994. Evolution of the Laacher See magma chamber: evidence from SIMS and TIMS measurements of U-Th disequilibria in minerals and glasses. Earth Planet. Sci. Lett. 126, 75–90.
Braunger, S., Marks, M.A.W., Walter, B.F., Neubauer, R., Reich, R., Wenzel, T., Parsapoor, A., Markl, G., 2018. The Petrology of the Kaiserstuhl Volcanic complex, SW Germany: the Importance of Metasomatized and Oxidized Lithospheric Mantle for Carbonatite Generation. J. Petrol. 59, 1731–1762.
Büchner, J., Tietz, O., Viereck, L., Suhr, P., Abratis, M., 2015. Volcanology, geochemistry and age of the Lausitz Volcanic Field. Int. J. Earth Sci. 104, 2057–2083.
Chen, L., Zheng, Y.-F., Zhao, Z.-F., 2018. A common crustal component in the sources of bimodal magmatism: Geochemical evidence from Mesozoic volcanics in the Middle-lower Yangtze Valley, South China. GSA Bull. 130, 1959–1980.
Corti, G., 2009. Continental rift evolution: from rift initiation to incipient break-up in the Main Ethiopian Rift, East Africa. Earth Sci. Rev. 96, 1–53.
Deering, C.D., Bachmann, O., Dufek, J., Gravley, D.M., 2011. Rift-Related transition from Andesite to Rhyolite Volcanism in the Taupo Volcanic Zone (New Zealand) Controlled by Crystal–melt Dynamics in Mush zones with Variable Mineral Assemblages. J. Petrol. 52, 2243–2263.
Dunworth, E.A., Wilson, M., 1998. Olivine Melilitites of the SW German Tertiary Volcanic Province: Mineralogy and Petrogenesis. J. Petrol. 39, 1805–1836.
Egli, D., Mosar, J., Ibele, T., Madritsch, H., 2017. The role of precursory structures on Tertiary deformation in the Black Forest—Hegau region. Int. J. Earth Sci. 106, 2297–2318.
von Engelhardt, W., Weiskirchner, W., 1961. Einführung zu den Exkursionen der Deutschen Mineralogischen Gesellschaft: zu den Vulkanschloten der Schwäbischen Alb und in den Hegau während der 39. Jahrestagung in Tübingen vom 11. bis 17. September 1961. Jahrestag. Deuts. Mineral. Gesellsch. 39, 1–24.
Frenzel, G., 1975. Die Nephelingesteinsparagenese des Katzenbuckels im Odenwald. In: Amstutz, G.C., Meisl, S., Nickel, E. (Eds.), Mineralien und Gesteine im Odenwald: Beiträge zum heutigen Forschungsstand. Heidelberg, pp. 213–228.
Freudenberg, W., 1906. Geologie und Petrographie des Katzenbuckels im Odenwald. Mitteilung. Grossherzogl. Badisch. Geol. Landesanst. 5, 185–344.
Freundt-Malecha, B., 2001. Plutonic rocks of intermediate composition on Gran Canaria: the missing link of the bimodal volcanic rock suite. Contrib. Mineral. Petrol. 141, 430–445.
Fuhrman, M.L., Lindsley, D.H., 1988. Ternary-feldspar modeling and thermometry. Am. Mineral. 73, 201–215.
Ghiorso, M.S., Gualda, G.A.R., 2015. An $H_2O$–$CO_2$ mixed fluid saturation model compatible with rhyolite-MELTS. Contrib. Mineral. Petrol. 169.
Ghiorso, M.S., Sack, R.O., 1995. Chemical mass transfer in magmatic processes IV. A revised and internally consistent thermodynamic model for the interpolation and extrapolation of liquid-solid equilibria in magmatic systems at elevated temperatures and pressures. Contrib. Mineral. Petrol. 119, 197–212.
Ginibre, C., Wörner, G., Kronz, A., 2004. Structure and Dynamics of the Laacher See Magma Chamber (Eifel, Germany) from Major and Trace Element Zoning in Sanidine: a Cathodoluminescence and Electron Microprobe Study. J. Petrol. 45, 2197–2223.
Gornitz, V., 1981. Skeletal crystals. In: Frye, K. (Ed.), The Encyclopedia of Mineralogy. Hutchinson Ross Publishing Company, Boston, MA, pp. 469–473.
Govindaraju, K., 1994. 1994 Compilation of Working Values and Sample Description for 383 Geostandards. Geostand. Newslett. 18, 1–158.
Green, T.H., Blundy, J.D., Adam, J., Yaxley, G.M., 2000. SIMS determination of trace element partition coefficients between garnet, clinopyroxene and hydrous basaltic liquids at 2–7.5 GPa and 1080–1200°C. Lithos 53, 165–187.
Gualda, G.A.R., Ghiorso, M.S., Lemons, R.V., Carley, T.L., 2012. Rhyolite-MELTS: a Modified Calibration of MELTS Optimized for Silica-rich, Fluid-bearing Magmatic Systems. J. Petrol. 53, 875–890.
von Hagke, C., Cederbom, C.E., Oncken, O., Stöckli, D.F., Rahn, M.K., Schlunegger, F., 2012. Linking the northern Alps with their foreland: the latest exhumation history resolved by low-temperature thermochronology. Tectonics 31, 1–25.
Hegner, E., Vennemann, T.W., 1997. Role of fluids in the origin of Tertiary European intraplate volcanism: evidence from O, H, and Sr isotopes in melilitites. Geology 25, 1035–1038.
Hoernle, K., Schmincke, H.-U., 1993. The Role of Partial Melting in the 15-Ma Geochemical Evolution of Gran Canaria: a Blob Model for the Canary Hotspot. J. Petrol. 34, 599–626.
Jung, S., Vieten, K., Romer, R.L., Mezger, K., Hoernes, S., Satir, M., 2012. Petrogenesis of Tertiary Alkaline Magmas in the Siebengebirge, Germany. J. Petrol. 53, 2381–2409.
Jung, S., Mezger, K., Hauff, F., Pack, A., Hoernes, S., 2013. Petrogenesis of rift-related tephrites, phonolites and trachytes (central European Volcanic Province, Rhön, FRG): Constraints from Sr, Nd, Pb and O isotopes. Chem. Geol. 354, 203–215.
Keller, J., Brey, G., Lorenz, V., Sachs, P., 1990. Volcanism and Petrology of the Upper Rhinegraben (Urach-Hegau-Kaiserstuhl). In: Urach, Hegau, Kaiserstuhl: Excursion 2A, August 27 to September 2, 1990. Mainz, pp. 1–60.
Kolb, M., Paulick, H., Kirchenbaur, M., Münker, C., 2012. Petrogenesis of Mafic to Felsic Lavas from the Oligocene Siebengebirge Volcanic Field (Germany): Implications for the Origin of Intracontinental Volcanism in Central Europe. J. Petrol. 53, 2349–2379.
Kong, W., Zhang, Z., Zhang, D., Wang, C., Santosh, M., Liu, B., Wei, B., 2023. New insights into deep carbon recycling and formation of nepheline-bearing alkaline rocks from Sr-Nd-Mg isotope compositions. GSA Bull. 135, 1530–1546.
Krause, O., 1969. Die Melilith-Nephelinite des Hegaus. Dissertation. Tübingen, p. 103.
Krause, O., Weiskirchner, W., 1981. Die Olivin-Nephelinite des Hegaus. Jahresh. Geol. Landes. Baden-Württemb. 23, 87–130.
Lacasse, C., Sigurdsson, H., Carey, S.N., Jóhannesson, H., Thomas, L.E., Rogers, N.W., 2007. Bimodal volcanism at the Katla subglacial caldera, Iceland: insight into the geochemistry and petrogenesis of rhyolitic magmas. Bull. Volcanol. 69, 373–399.
Le Bas, M.J., 1987. Nephelinites and carbonatites. Geol. Soc. Lond. Spec. Publ. 30, 53–83.
Lexa, J., Seghedi, I., Németh, K., Szakács, A., Konečny, V., Pécskay, Z., Fülöp, A., Kovacs, M., 2010. Neogene-Quaternary Volcanic forms in the Carpathian-Pannonian Region: a review. Cent. Eur. J. Geosci. 2, 207–270.
Mahfoud, R.F., Beck, J.N., 1989. Alkaline basalt-phonolite rocks from the Singen area, Hegau, southern F.R.G. Chem. Geol. 74, 217–227.
Mann, U., Marks, M.A., Markl, G., 2006. Influence of oxygen fugacity on mineral compositions in peralkaline melts: the Katzenbuckel volcano, Southwest Germany. Lithos 91, 262–285.
Mäussnest, O., Schreiner, A., 1982. Karte der Vorkommen von Vulkangesteinen im Hegau. Abhandl. Geol. Landes. Baden-Württemb. 10, 1–48.
Mayer, B., Jung, S., Romer, R.L., Stracke, A., Haase, K.M., Garbe-Schönberg, C.D., 2013. Petrogenesis of Tertiary Hornblende-bearing Lavas in the Rhön, Germany. J. Petrol. 54, 2095–2123.
Mourey, A.J., France, L., Ildefonse, B., Gurenko, A., Laporte, D., 2023. Genesis of Carbonatite at Oldoinyo Lengai (Tanzania) from Olivine Nephelinite: Protracted Melt Evolution and Reactive Porous Flow in Deep Crustal Mushes. J. Petrol. 64, egad084.
Palme, H., O'Neill, H., 2014. Cosmochemical estimates of Mantle Composition. In: Holland, H.D., Turekian, K.K. (Eds.), The Mantle and Core, 2nd ed. Elsevier, Amsterdam, Heidelberg, pp. 1–39.
Panina, L.I., Sharygin, V.V., Keller, J., 2000. Olivine nephelinite, tephrite, essexite, phonolite, and tinguaite from Kaiserstuhl, Germany: evidence from melt inclusions in pyroxene. Geochem. Int. 38, 343–352.
Peccerillo, A., Barberio, M.R., Yirgu, G., Ayalew, D., Barbieri, M., Wu, T.W., 2003. Relationships between Mafic and Peralkaline Silicic Magmatism in Continental Rift Settings: a Petrological, Geochemical and Isotopic Study of the Gedemsa Volcano, Central Ethiopian Rift. J. Petrol. 44, 2003–2032.
Peccerillo, A., Donati, C., Santo, A.P., Orlando, A., Yirgu, G., Ayalew, D., 2007. Petrogenesis of silicic peralkaline rocks in the Ethiopian rift: Geochemical evidence and volcanological implications. J. Afr. Earth Sci. 48, 161–173.
Pfänder, J.A., Jung, S., Münker, C., Stracke, A., Mezger, K., 2012. A possible high Nb/Ta reservoir in the continental lithospheric mantle and consequences on the global Nb budget – evidence from continental basalts from Central Germany. Geochim. Cosmochim. Acta 77, 232–251.

Prowatke, S., Klemme, S., 2005. Effect of melt composition on the partitioning of trace elements between titanite and silicate melt. Geochim. Cosmochim. Acta 69, 695–709.
Przybyla, T., Pfänder, J.A., Münker, C., Kolb, M., Becker, M., Hamacher, U., 2018. High-resolution $^{40}Ar/^{39}Ar$ geochronology of volcanic rocks from the Siebengebirge (Central Germany)—Implications for eruption timescales and petrogenetic evolution of intraplate volcanic fields. Int. J. Earth Sci. 107, 1465–1484.
Ring, U., Bolhar, R., 2020. Tilting, uplift, volcanism and disintegration of the south German block. Tectonophysics 795, 228611.
Rooney, T., Furman, T., Bastow, I., Ayalew, D., Yirgu, G., 2007. Lithospheric modification during crustal extension in the Main Ethiopian Rift. J. Geophys. Res. Solid Earth 112. B10201.
Rooney, T.O., 2020. The Cenozoic magmatism of East Africa: Part II – Rifting of the mobile belt. Lithos 360-361, 105291.
Schleicher, H., Keller, J., Kramm, U., 1990. Isotope studies on alkaline volcanics and carbonatites from the Kaiserstuhl, Federal Republic of Germany. Lithos 26, 21–35.
Schmitt, A.K., Wetzel, F., Cooper, K.M., Zou, H., Wörner, G., 2010. Magmatic Longevity of Laacher See Volcano (Eifel, Germany) Indicated by U–Th Dating of Intrusive Carbonatites. J. Petrol. 51, 1053–1085.
Schmitt, A.K., Klitzke, M., Gerdes, A., Schäfer, C., 2017. Zircon Hafnium–Oxygen Isotope and Trace Element Petrochronology of Intraplate Volcanic Rocks from the Eifel (Germany) and Implications for Mantle versus Crustal Origins of Zircon Megacrysts. J. Petrol. 58, 1841–1870.
Schreiner, A., 2008. Hegau und westlicher Bodensee, 3rd ed. Borntraeger, Berlin, Stuttgart, p. 90.
Sharygin, V.V., Di Muro, A., Madyukov, I.A., 2005. Crystallization Temperature of Haüyne from Phonolite (ULST, E.Eifel, Germany) and Haüynophyre (Vulture volcano, Italy): Evidence from Silicate Melt Inclusions. Abstract E-book of ECROFI 18.
Sliwinski, J.T., Bachmann, O., Ellis, B.S., Dávila-Harris, P., Nelson, B.K., Dufek, J., 2015. Eruption of shallow crystal cumulates during explosive phonolitic eruptions on Tenerife, Canary Islands. J. Petrol. 56, 2173–2194.
Staesche, A., 1995. Der genetische Zusammenhang zwischen Melilithiten und Phonolithen des Hegaus, SW-Deutschland (Diploma thesis). Tübingen, p. 66.
Stähle, V., Koch, M., 2003. Primary and secondary pseudobrookite minerals in volcanic rocks from the Katzenbuckel Alkaline complex, southwestern Germany. Swiss Bull. Mineral. Petrol. 83, 145–158.
Stock, M., 1990. Mikrothermometrische Untersuchung der Fluid- und Schmelzeinschlüsse in Olivinen der Nephelinite vom Neuhewen und Hohenstoffeln (Hegau). Diploma thesis. Tübingen, p. 86.
Tamura, Y., Tatsumi, Y., 2002. Remelting of an Andesitic Crust as a possible Origin for Rhyolitic Magma in Oceanic Arcs: an example from the Izu-Bonin Arc. J. Petrol. 43, 1029–1047.
Theilen-Willige, B., 2011. Remote sensing and GIS studies of the Hegau Volcanic Area in SW Germany. Photogram. – Fernerkund. – Geoinform. 2011, 361–372.
Trua, T., Deniel, C., Mazzuoli, R., 1999. Crustal control in the genesis of Plio-Quaternary bimodal magmatism of the Main Ethiopian Rift (MER): geochemical and isotopic (Sr, Nd, Pb) evidence. Chem. Geol. 155, 201–231.
Ulrych, J., Lloyd, F.E., Balogh, K., 2003. Age Relations and Geochemical Constraints of Cenozoic Alkaline Volcanic Series in W Bohemia: a Review. GeoLines 15, 168–180.
Ulrych, J., Lloyd, F.E., Balogh, K., Hegner, E., Langrová, A., Lang, M., Novák, J.K., Řanda, Z., 2005. Petrogenesis of alkali pyroxenite and ijolite xenoliths from the Tertiary Loucna–Oberwiesenthal Volcanic Centre, Bohemian Massif in the light of new mineralogical, geochemical, and isotopic data. Neues Jahrb. Mineral. - Abhandlung. (J. Mineral. Geochem.) 182, 57–79.
Ulrych, J., Dostal, J., Adamovič, J., Jelínek, E., Špaček, P., Hegner, E., Balogh, K., 2011. Recurrent Cenozoic volcanic activity in the Bohemian Massif (Czech Republic). Lithos 123, 133–144.
Vaněčková, M., Holub, F.V., Souček, J., Bowes, D.R., 1993. Geochemistry and petrogenesis of the tertiary alkaline volcanic suite of the Labe tectonovolcanic zone, Czech Republic. Mineral. Petrol. 48, 17–34.
Wilson, M., Downes, H., Cebriá, J.-M., 1995a. Contrasting fractionation trends in coexisting Continental Alkaline Magma Series; Cantal, Massif Central, France. J. Petrol. 36, 1729–1753.
Wilson, M., Rosenbaum, J.M., Dunworth, E.A., 1995b. Melilitites: partial melts of the thermal boundary layer? Contrib. Mineral. Petrol. 119, 181–196.
Wimmenauer, W., 1974. The Alkaline Province of Central Europe and France. In: Sørensen, H. (Ed.), The Alkaline Rocks, pp. 238–271.
Wörner, G., Schmincke, H.-U., 1984. Petrogenesis of the Zoned Laacher See Tephra. J. Petrol. 25, 836–851.
Wörner, G., Wright, T.L., 1984. Evidence for Magma mixing within the Laacher See Magma Chamber (East Eifel, Germany). J. Volcanol. Geotherm. Res. 22, 301–327.
Zaitsev, A.N., Marks, M., Wenzel, T., Spratt, J., Sharygin, V.V., Strekopytov, S., Markl, G., 2012. Mineralogy, geochemistry and petrology of the phonolitic to nephelinitic Sadiman volcano, Crater Highlands, Tanzania. Lithos 152, 66–83.
Zhao, K., Xu, X., Bachmann, O., Nan, T., Xia, Y., 2023. $H_2O$-controlled eruptive filtering on the bimodality of Continental Volcanism across tectonic settings. J. Petrol. 64, egad006.
Zou, H., Zindler, A., 1996. Constraints on the degree of dynamic partial melting and source composition using concentration ratios in magmas. Geochim. Cosmochim. Acta 60, 711–717.